University of Texas at El Paso
DigitalCommons@UTEP

Open Access Theses & Dissertations

2012-01-01

Dynamic Earthquake Triggering in the Continental U.S.

Ibrahim Cerda
University of Texas at El Paso, ibrahimc@hotmail.com

Follow this and additional works at: https://digitalcommons.utep.edu/open_etd

 Part of the Geophysics and Seismology Commons

Recommended Citation
Cerda, Ibrahim, "Dynamic Earthquake Triggering in the Continental U.S." (2012). *Open Access Theses & Dissertations*. 2055.
https://digitalcommons.utep.edu/open_etd/2055

This is brought to you for free and open access by DigitalCommons@UTEP. It has been accepted for inclusion in Open Access Theses & Dissertations by an authorized administrator of DigitalCommons@UTEP. For more information, please contact lweber@utep.edu.

DYNAMIC EARTHQUAKE TRIGGERING IN THE CONTINENTAL U.S.

IBRAHIM CERDA

Department of Geological Sciences

APPROVED:

Aaron A. Velasco, Ph.D., Chair

Laura L. Serpa, Ph.D.

Virgilio Gozalez, Ph.D.

Benjamin C. Flores, Ph.D.
Dean of the Graduate School

Copyright ©

by

Ibrahim Cerda

2012

Dedication

I lovingly dedicate this thesis to my daughter, Madyson R Cerda.
My little angel.

To my parents, Jose L.Cerda and Elvia Solis de Cerda.
For all their support and guidance in my academic endeavors

DYNAMIC EARTHQUAKE TRIGGERING IN THE CONTINENTAL U.S.

by

IBRAHIM CERDA, B.S.E.E., B.S.E.SCI.

THESIS

Presented to the Faculty of the Graduate School of

The University of Texas at El Paso

in Partial Fulfillment

of the Requirements

for the Degree of

MASTER OF SCIENCE

Department of Geological Sciences

THE UNIVERSITY OF TEXAS AT EL PASO

December 2012

Acknowledgements

I would like to thank Dr. Aaron A. Velasco, my committee chairman and advisor, for his constant support and unconditional help. I would also like to thank all my colleagues and friends for all the ups and downs while we were doing our master studies. All of them contributed in so many different ways to make this dream come true. Last, but not least, I would like to thank all the people that are part of the Geological Department at UTEP, with their help and support this Master Thesis became a reality.

Thanks to all.

Abstract

Seismological studies have classified the changes in field stress required to trigger remote earthquakes into two basic types: static and dynamic triggering. Static triggering mainly originates from geological faults already present in certain tectonic environments and they could be originated due to continental crust, subduction zones or even from a highly seismicity zone. Dynamic triggering occurs when an event (earthquake) has been induced by the passing of seismic waves from a large main shock located at least two or more fault lengths from the epicenter of the main shock. This study investigates details of dynamic triggering not seen in previous studies. This investigation focuses on gathering and analyzing data to detect and tabulate high-frequency detections (HFD) that might indicate locally triggered earthquakes on the United States continent. In particular, data in form of seismic waveforms was downloaded and collected from EarthScope's USArray, which has an active Transportable Array (TA) station program that emphasizes the broadband compilation of geophysical data across the continental U.S. All seismic waveforms were gathered using ~400 different seismic stations primarily focusing on two types of data: local events with a magnitude M≥4.0, and teleseismic events with magnitude M≥6.5. Triggered events were identified inherent in the event's frequency spectra using an automated detector (Antelope software) and a series of filters by examining both the amplitude and frequency of the waves responsible for triggering. The results will help provide for a better understanding of the physical mechanisms involved in dynamic earthquake triggering and also will help identify zones in the U.S. continent which may be more susceptible to these kinds of events.

Table of Contents

List of Tables

List of Figures

Chapter 1: Introduction

The sudden release of energy in the Earth, known as earthquakes, generate seismic waves, which not only take lives and damage man-made structures depending on the magnitude and location, but also produce secondary effects, most often in the form of a tsunami, or tidal wave.

Body waves are seismic waves that propagate through the body of earth. These include *P*-waves (primary/compressional waves), which propagate fastest and are longitudinal, and *S*-waves (secondary/shear waves), which move somewhat less fast and are transverse.

Surface waves are seismic waves that propagate along the surface of earth. These waves tend to be slower and more destructive than body waves because of their long frequency, long duration and large amplitude. Examples include Rayleigh waves (waves with both transverse and longitudinal characteristics) and Love waves (purely longitudinal). These waves have been shown to trigger earthquakes at great distances from a large earthquake, a process called remote or dynamic triggering.

A growing body of evidence demonstrates that dynamic stresses propagating as seismic waves from large earthquakes are capable of triggering additional earthquakes ranging from aftershocks in the near-field (within one to two source dimensions of the main shock epicenter) to remotely triggered earthquakes at distances exceeding 10,000 km.

Different hypotheses exist to explain the question of how, why and when dynamic triggering of earthquakes occurs. For example, static and dynamic Coulomb failure stress has been proposed to predict the timing and location of future aftershocks and rupture lengths based on fault geometry (Harris et al., 1998; Hill et al., 1993; Gomberg et al., 2004). This approach cannot fully explain long time delays between other events derived from the main shock because the majority of faults do not have a large history of seismicity to make such analysis (Harris, 1993). Static and dynamic rate and state stress defined in laboratory experiments have been conducted, yet actual fault values and geodetic data have not been well established to support these laboratory experiments (Harris, 1998). Fluid flow may explain

time delays between main shock and subsequent events (called delayed triggering), but may not be successful at predicting both the spatial and temporal aftershock pattern (Li et al., 2002; Seeber et al., 1998).

Surface waves appear to be the main triggering disturbance (Hill, et al., 2008; West et al., 2005; Velasco, et al., 2008). An important feature of surface waves are their propagation effects such as radiation pattern, geometrical spreading factors, attenuation and dispersion (waves of different periods travel at different velocities). Surface waves also travel through the earth at different velocities, group and phase, which are related by a derivative and where the group velocity will map the peak amplitudes as a function of period (Velasco, 2010). As a result, the surface waves' arrivals must not be considered to be sharp arrivals, but spread out energy in time with a very specific surface wave's group and phase velocities depending on the geological setting.

Dynamic triggering has not been fully studied or understood because it is relatively new phenomena, there are a small number of seismometers station locations with large bandwidth and dynamic ranges, and there are just a few earthquake catalogs that are complete to low magnitudes.

This investigation focuses on gathering and analyzing data to detect and tabulate high-frequency detections (HFD) that might indicate locally triggered earthquakes on the United States continent.

Chapter 2: Static versus Dynamic Triggering

Seismological studies have classified the variation of field stresses into two types: static stress and dynamic stress (e.g., Velasco, 2008; Brodsky, 2000). Static triggering figure 2.1(a), originates from slip-induced movement along geological faults. Static triggering occurs near a main shock rupture, due to the permanent stress change produced by one earthquake. Because static stress changes decay relatively rapidly with distance, the triggering potential caused by static stress is generally limited to one or two fault lengths from a given epicenter.

Dynamic triggering figure 2.1 (b), on the contrary, occurs beyond the influence of static stresses and usually correlates with the passage of large amplitude and long duration passing signals, such as surface waves. Current evidence suggests that triggering of events can occur at large distances away (thousands of km) from the original main earthquake (e.g., Velasco et al., 2008; Brodsky et al., 2000; Tibi et al., 2003; Husen et al., 2004). If we assume that distant earthquakes were not affected by static stress changes from a main event, these events can be classified as dynamically and/or remotely triggered events by the seismic signal of the main shock.

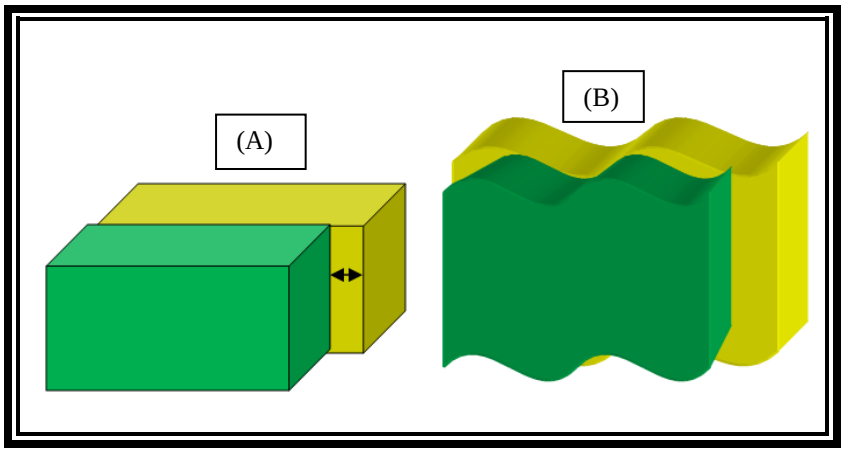

Figure 2.1: Diagram illustrating the two types of stresses. (A) Static stress caused by natural stresses associated with the fault. (B) Dynamic stress produced by the passing of surface waves.

Dynamic triggering does not appear to depend on the magnitude of the trigger nor distance from the event, but could be a function of the oscillating stress frequency (Velasco et al., 2008). Surface waves can efficiently trigger earthquakes, more than any other seismic phases (Parsons and Velasco, 2008). Dynamic stresses can have much larger amplitude relative to the state changes to alter fault zone properties more effectively in ways that permit a range of time delays between triggering (Brodsky, 2000). Dynamic triggering requires large amplitude seismic waves, such as surface waves, yet a specific threshold along with different frequency ranges may be needed to trigger earthquakes at greater distances away from the main shock. Triggering caused by surface waves can be correlated with crack growth (Brodsky et al., 2000); the presence of fluid flow on certain zones and its dependency with Coulomb stresses (Brodsky et al., 2003). Most important, frequencies and amplitudes of seismic waves could also be associated to triggering of certain events (Brodsky et al., 2005). Also, the orientations of the seismic waves with respect to the local fault geometry are more likely to trigger distance aftershocks (Hill, 2008; Gonzalez-Huizar and Velasco, 2010).

Changes in the mechanical properties or failure processes of a fault do not mean that failure occurs immediately with the passing of the seismic waves. In some cases, a delay may occur. For this reason, there may be a difference in time delay between triggering and triggered earthquakes (Kilb et al., 2000). Furthermore, not all large earthquakes trigger remote seismicity and certain geographic regions appear more susceptible to triggering (Kilb et al., 2000). Subsequently, the time delay between trigger and triggered event may depend on how close the fault was to failure. Time/stress path dependence of failure cannot be represented with a Coulomb failure model (which predicts failure at a particular stress state, independent of rate or time). Permanent stress changes can also contribute to the alteration of fault zone properties, but in this case, these stress changes, could be related more to the proximity of the main shock rupture and not directly connected to dynamic triggering.

Many scientific questions remain about dynamic triggering, including how far from the main event does triggering occur, is there a stress threshold for triggering, does orientation of the passing seismic waves contribute to the triggering stresses, and is there a frequency dependence on triggering potential? This thesis focuses on further analyzing dynamic triggering to study some of these questions.

Chapter 3: Dynamic Earthquake Triggering-Proof of Existence

Dynamic triggering has been widely studied for the past few years. Figure 3.1, shows an example of a triggered event produced by the 11 March, 2011 Japan earthquake. There are three events that show the existence of dynamic triggering. Those events are the 1992 Landers earthquake, the 1999 Hector Mine earthquake and the 2002 Denali Fault earthquake, Alaska.

3.1 LANDERS EARTHQUAKE

.

28 June 1992. The magnitude 7.3 Landers earthquake ruptured a 70 km length of the Mojave Desert in southern California (Anderson et al., 1994; Hill et al., 1993). Documented seismicity rate increases began within minutes to 33 hours following the main shock (Harris, 1998).

Seismicity rates increased and were recorded at a number of sites across western North America at distances ranging from 200 to as much as 1250 km (17 source dimensions) (Hill et al., 1993). These sites included Long Valley caldera, Lassen Peak, Burney, Ca, the Wasatch front in central Utah, Cascade Idaho, and Yellowstone National Park (Hill et al., 1993).

The Landers main shock resulted in a unilateral rupture propagating to the north-northwest along a series of north-northwest striking dextral fault segments (Gomberg et al., 2001). All of the recognized sites of dynamic triggering were north of the Landers epicenter (Gomberg et al., 2001), suggesting that amplification enhanced by rupture directivity may influence the distribution of dynamic triggering (Hill et al., 1993).

The observed beginning of activity at each site is consistent with an instantaneous increase in local seismicity rate at the time of the Landers main shock.

3.2 HECTOR MINE EARTHQUAKE

16 October 1999. The magnitude 7.1 earthquake ruptured a 40 km length with a fault rupture that was bilateral but with the dominant rupture direction to the south-southeast of the epicenter (Gomberg et al., 2001).

The beginning of the triggered seismicity coincided with arrival of the surface waves from the Hector Mine earthquake (Gomber et al., 2001). The most energetic triggered response to the Hector Mine dynamic stresses was in Salton Trough south of the epicenter (Gao et al., 2000).

Seismicity rates increased and were recorded at a number of sites southeast at distances ranging from ~87 km at the vicinity of Indio to ~750 km at the Geysers geothermal field (Gomberg et al., 2001). The time delayed recorded by triggering rates range from ~20 minutes at Mammoth Mountain (~450 km from epicenter) to ~2 hours at Cierro Prieto (~250 km from epicenter) (Gomberg et al., 2001).

3.3 DENALI FAULT EARTHQUAKE

3 November 2002. This earthquake produces the most extensively recorded remote dynamic triggering. The Denali Fault earthquake was centered 65 km east of Denali National Park, (Alaska) and it was represented by a complex rupture with surface displacement at a maximum of 8.8 meters (Eberhart-Phillips et al., 2003).

The beginning of dynamic triggering developed as a seismicity rate increase during passage of the Love and Rayleigh waves (Husen et al., 2004). All dynamic triggering events recorded were located southeast of the epicenter (Husen et al., 2004).

The time delayed recorded by triggering rates range from ~2.5 hours at Mount Rainer (central Washington, ~3108 km from epicenter) to ~8 days at Yellowstone, Wyoming (~3100 to 3150 km from epicenter) (Pankow et al., 2004). The Denali Fault event triggered dynamically earthquake activity

recorded at distances as great as 3660 km in southeastern California (Coso geothermal field) (Eberhart-Phillips et al., 2003).

The initial activity recorded was ~130 earthquakes occurring in spasmodic burst during the first four hours. Seismicity slowed to ~35 events per day after a few days, but continued to occur for at least ten days (Eberhart-Phillips et al. 2003). Yellowstone produced the most active response (Husen et al., 2004).

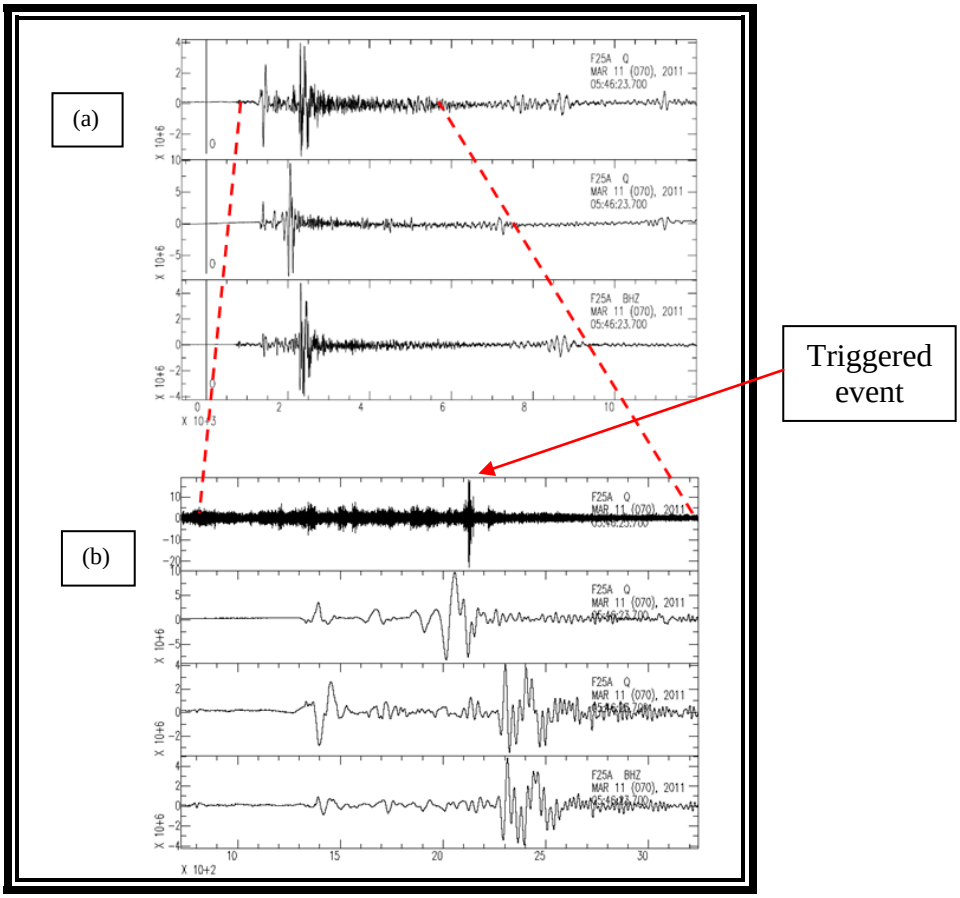

Figure 3.1: (a) Seismogram recorded at station F25A in Bowman, SD, USA for the 11 March, 2011, Japan Earthquake (Mw=9.0). (b) Same seismogram window high-pass filtered at a frequency of 5 Hz, showing a zoom-in of the high-pass filtered record indicating the presence of a triggered event inherent under the same seismic signal.

Chapter 4: Data

Data was collected from the EarthScope USArray program funded by the National Science Foundation and operated by the Incorporated Research Institutions for Seismology (IRIS). The EarthScope USArray has deployed a rolling array of 450 Transportable Array (TA) seismic stations, 70 km grid spacing, all over the North American continent. The main goal of USArray is to collect all broadband data to generate a seismological and geophysical database that describes in detail the structure of the subsurface and at the same time, make all these information public to the scientific community. The +450 TA's stations are moving from West to East with the purpose of covering every part of the U.S. over the 10 years of the project, and each station records for two years before it is moved. For each event recorded, the TA network is in a slightly different position. Each TA station is composed of a three-component broadband seismometer that records in real time and the data is stored and readily accessible using IRIS databases.

Data is composed of two segments. Segment one, initial analysis, is composed of seismograms of $4.0 \leq M \leq 7.5$ of all the events that have been recorded in the U.S. by three reference seismic stations. This segment is intended to generate a threshold to be implemented as part of our algorithm. Segment two, feature analysis, is composed of five events; three teleseismic megatrust events: the Maule, Chile on February 27, 2010 (M 8.8), Tohoku-Oki, Japan on March 11, 2011 (M 9.0), West coast of northern Sumatra on April 11, 2012 (M 8.2 and M 8.6); and two large regional events, the Baja California, Mexico on April 04, 2010 (M 7.2) earthquake, and the Wells Nevada, U.S., on February 21, 2008 (M 6.0). Segment two, is the process of implementing this threshold value into an algorithm suitable of detecting triggered events after the passing of surface waves.

Chapter 5: Software Required

5.1 SOD

Standing Order for Data (SOD), created by the University of South Carolina, is a powerful and flexible Data Handling Interface (DHI) data request utility. SOD automates selection and downloading of earthquake data and allows the user to define data gathers based on earthquake magnitude, the location of earthquakes and recording stations, and the time bias around specific seismic phase arrivals.

SOD, in the form of an XML file (Recipe) (Appendix A), specifies the earthquakes, channels and seismograms of interest. SOD repeatedly checks DHI event catalog services from a number of data centers and acts on earthquakes that match to the standing order. Once this occurs, SOD then contacts the DHI waveform services from these data centers and follows the standing order instructions as to the stations, channels and time parameters requested in order to collect data that the user wants. The data is transferred to the user's computer in an automated fashion. SOD is capable of post-processing operations on the data stream such as mean removal, saving data to a SAC or miniSEED file.

5.2 SAC

Seismic Analysis Code (also known as SAC2000), is a signal processing and analysis code that has been developed by Lawrence Livermore National Laboratory (LLNL) over the past 25 years for a variety of seismic and geophysical research projects. SAC is an interactive program designed for the study of sequential signals, especially time-series data. Emphasis has been placed on analysis tools used by research seismologist in the detail study of seismic events. Analysis capabilities include general arithmetic operations, Fourier transforms, three spectral estimation techniques, IIR and FIR filtering, signal stacking, decimation, interpolation, and seismic phase picking. SAC also contains an extensive graphics capability.

SAC is used extensively by the seismic community because it has a broad range of well-tested, efficient data analysis capabilities (examples include: data inspection, phase picking, signal correction,

quality control, binary data operations, travel-time analysis, spectral analysis including high-resolution spectral estimation, spectrograms and binary sonograms, and array and three-component analysis). It is reliable and easy to use, has a macro programming language that allows users to develop innovative new analysis techniques. Figure 5.1(a), shows an example of an event using SAC software.

5.3 ANTELOPE

Boulder Real Time Technologies, Inc. (BRTT) provides the Antelope software package. Antelope is a system of software modules that implement acquisition, transport, buffering, processing, archiving and distribution of environmental monitoring information. It is an integrated collection of programs for data collection and seismic data analysis, and typically runs at the central processing site. The data are stored in a flat file CSS3.0 style database, which allows for processing large amounts of data.

Antelope has an open architecture, with extensive documentation of internal interfaces. The Antelope real time system is built around a large, flexible, non-volatile ring buffer. Data acquisition modules communicate with data loggers, and leave data on the ring buffer. The ring buffer protocol provides a convenient method for directly importing data from the other sites, as well as exporting data. For instance, the detector reads data from the ring buffer and writes detections to the orb. The grid associator reads the detections and quickly provides preliminary event locations. This architecture facilitates running multiple detectors or associators, and other refinements. Figure 5.1 (b), shows an example of an event using Antelope software.

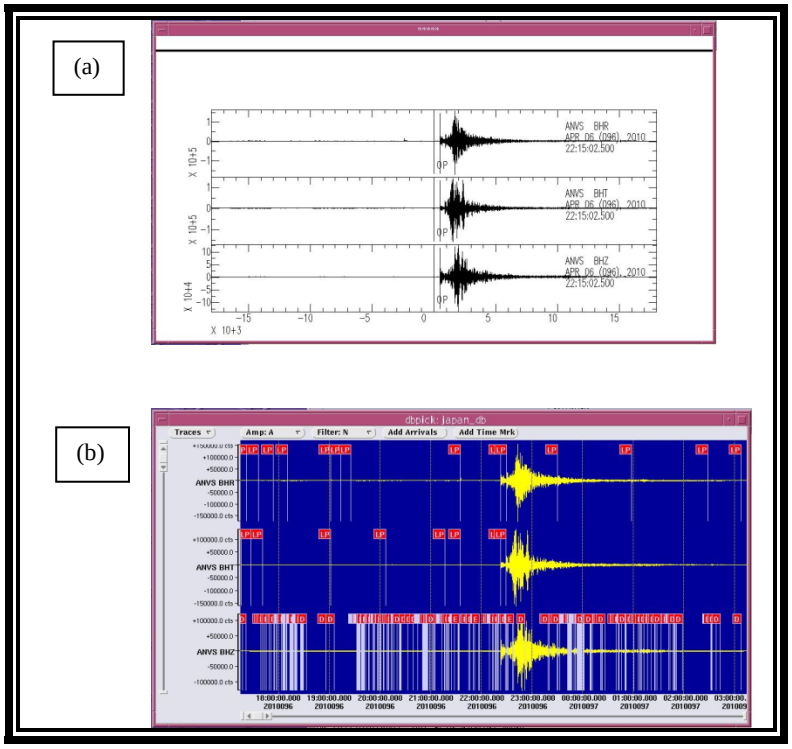

Figure 5.1: (a) Seismograms from the Japan Earthquake **(**East coast of Honshu, Japan M 9.0, March 11, 2011) displaying its three components (R, T, Z). (a) Seismogram recorded at ANVS station (KYRGYZ Network), analyzed using sac2000 software. (b) Same seismogram as in (a) but now using Antelope software, indicating all STA/LTA detections.

Chapter 6: Methodology

6.1 TRIGGERING DETECTION

For each of the five seismic events main shock, at each station, an automated search for high frequency detections (HFD) that potentially indicate a remotely triggered earthquake have been applied. Antelope software, have give us the opportunity to explore different automatic detection algorithms focusing on developing a suitable detector that can identify events or spurious detections and other possible high frequency noise. The procedure was to acquire the require information, generate Antelope database files, apply a STA/LTA algorithm, high pass filter the seismograms and finally, analyze the results in order to identify all potential detections that could be associate with dynamic triggering.

6.2 SHORT TERM AVERAGE/LONG TERM AVERAGE

The Short Term Average/Long Term Average (STA/LTA) (Appendix B), is the ratio between the amplitude, computed as the norm (average of the absolute values), of the signal on a short time window of length STA and on a long time window of length LTA. At a given point STA/LTA is computed for the time windows preceding the point. For the first signal points, where there are not enough preceding data points to compute the complete LTA and/or STA, the average of the whole signal is used for the missing points. The STA/LTA will detect on one or more channels of the waveform data and write the detection inside an output database. For each channel of the database, Antelope can run multiple detections, on the same channel of the data with different frequency passbands. The implementation of a STA/LTA was used in early seismological applications to decrease the computation time. It does not modify the results and can effectively produce threshold values gather from all detectors run.

6.3 SIGNAL FILTERING

Seismograms were analyzed utilizing a time window of 5 hours before and 10 hours after the main shock of the event. This specific range of time before and after the event, allow for the opportunity to apply to the signal a high-pass filter (~5 Hz) to identify if any event have been 'hidden' into the primary surface wave, as illustrated in Figure 3.1 (e.g., Velasco et al., 2008). Applying a 5 Hz high-pass filter to seismograms enhances the local earthquakes for detection of possible triggered events. It efficiently eliminates long period surface waves, eliminates the main shock coda waves at distances beyond 500 km and also eliminates other high-frequencies signals, like noise.

6.4 IDENTIFICATION OF TRIGGERED EVENTS

To identify possible triggered events, all HFD's have been added along the group velocities curves for Love and Rayleigh waves. We have created histograms for detections using bins of peak amplitudes with a window of 300 seconds (Velasco et al., 2008). By using this procedure, it is expected to see evidence of delayed dynamic triggering from the arrival of Love and Rayleigh waves. To qualitatively identify whether the increase in HFD's is significant and to correlate the passage of seismic energy from the main shock, each waveform that has been identified as a potential triggered event was analyzed in amplitude and frequency.

Chapter 7: Analysis and Results

7.1 SEGMENT ONE. INITIAL ANALYSIS

Initial data is composed of seismograms recorded in the U.S. continent by three reference stations as described in Table 7.1, in order to explore our detectors (STA/LTA) to make sure we are detecting local events. This set of seismograms waveforms were downloaded for local events with a distance range of ≥1000 km from each station, using a time frame from January 01 to December 31, 2007. Thus, we analyze 1 year of continuous data.

Table 7.1: Seismic Network Information summarizing reference stations parameters.

NETWORK STATIONS				
STATION	**NETWORK**	**LOCATION**	**LATITUDE**	**LONGITUDE**
ANMO	IU	Albuquerque, NM	34.95	-106.46
R11A	TA	Troy Canyon, NV	38.35	-115.59
TX31	IM	Lajitas, TX	29.33	-103.67

Data is composed of ~1000 seismograms for each respectively station. All information was requested to IRIS using SOD, and stored in the Geological Science Department data servers. All waveforms were analyzed using SAC software. Information gathered from SOD comes with a specific extension. It was necessary to convert from SOD to SAC extension in order to be executed and analyzed by SAC software. We then created the Antelope database. Once the information is readable by SAC and Antelope, all seismograms were analyzed visually to detect and sort cleanest signals. Not all seismograms were useful and it was necessary to remove bad traces with incomplete or noisy surface wave recording, in some cases, the presence of excessive noise might interfere with an accurate reading. Approximately, +1000 seismograms were analyzed.

We explore the duration of local to teleseismic signals for our STA/LTA detector by calculating the energy envelope of our signals. To obtain the envelope of every signal, the Hilbert transform was implemented as part of the macro mentioned before. The Hilbert transform can be considered to be a filter that simply shifts phases of all frequencies components of its input by –n/2 radians. One of SAC applications allows us to implement a macro in order to reproduce the envelope of the analytic signal for a better visualization and interpretation. The SAC macro could be found in Appendix C. A complex time signal (analytic signal) can be constructed from a real valued input signal by adding the input signal and the Hilbert transform of the original input signal. From the result, the amplitude of the analytic signal is considered to be the enveloped of the signal. Figure 7.1 shows an example of a seismic waveform and its envelope package.

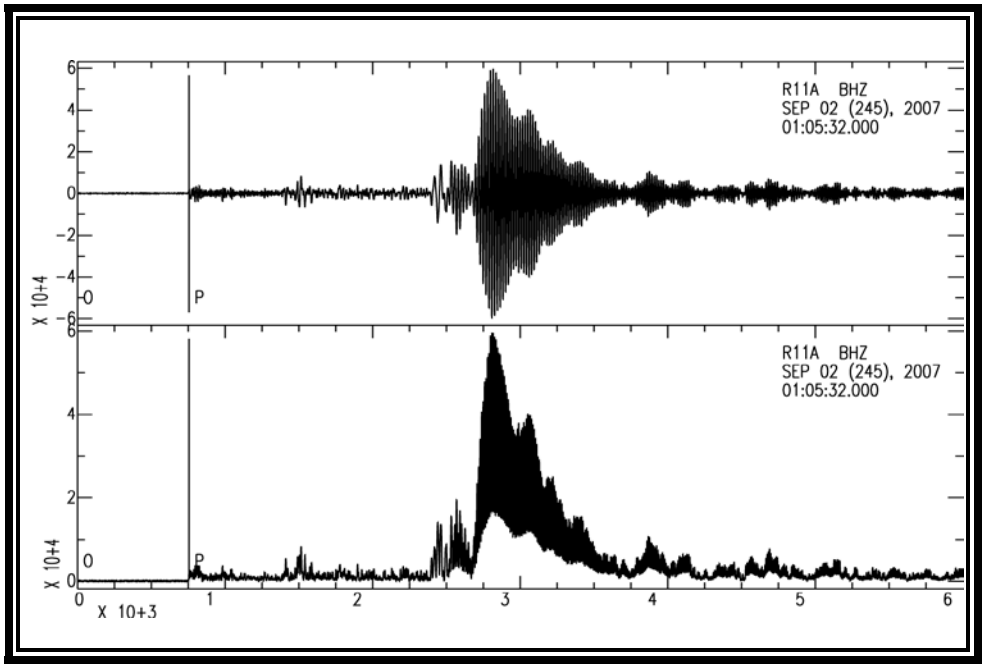

Figure 7.1: Seismogram and its envelope signal. Event recorded at station R11A on September 02, 2007 at 01:05:18 UTC. Santa Cruz Islands. Mag. 7.2

In order to obtain the signal time duration, the waveforms were analyzed by measuring two different parts of the signal, one from the beginning of the P-wave (T1) to the end of the surface wave (T2) and a second measurement, for the complete surface wave (T3-T4), as shown in Figure 7.2. Coda measurements were eliminated from this approach due to the fact that only the values of the main signal spectra were intended to give a more accurate threshold values. We are using the different duration to explore the STA/LTA parameters to use for our analysis.

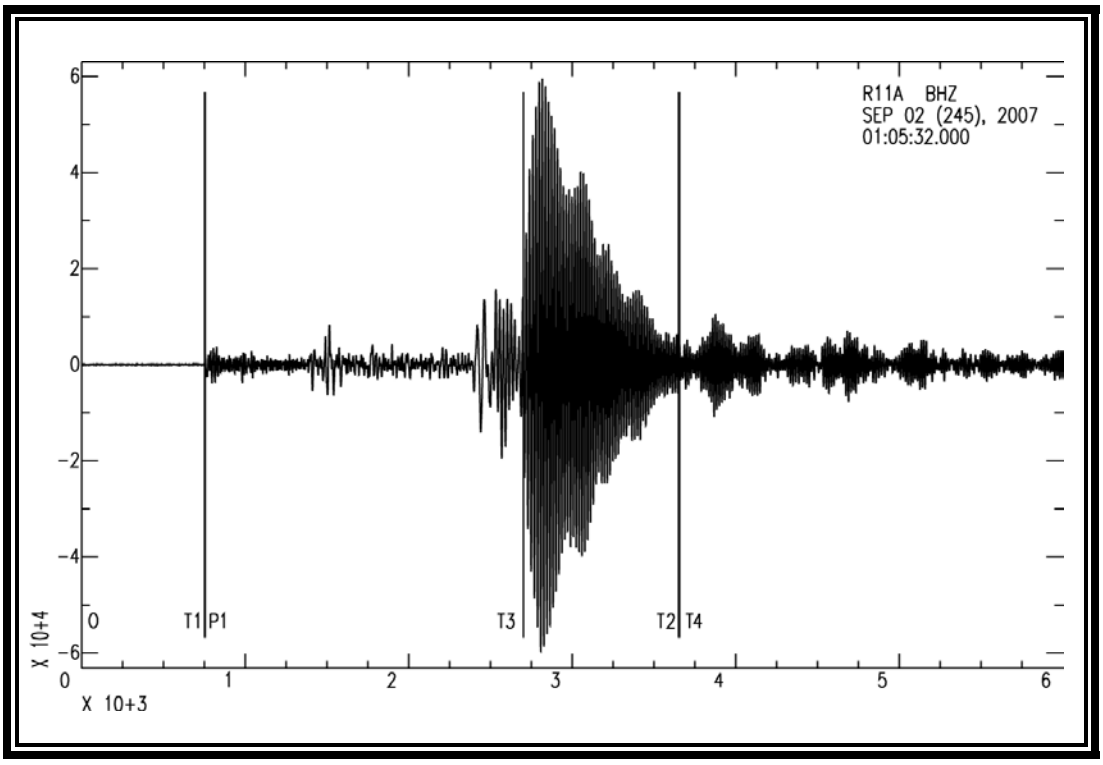

Figure 7.2: Seismogram showing signal time duration. Beginning of P (T1) to end surface wave (T2). Beginning of surface wave (T3) to end surface wave (T4)

7.1.2 STA/LTA Algorithm

The results gathered from analyzing all the previous seismic waveforms has given us the opportunity to developed different set of parameters. We used the Antelope software, to develop and test an automated detection algorithm. Table 7.2 shows the initial set of parameters, D and E, implemented as part of the STA/LTA algorithm at the beginning of this project. The STA/LTA algorithm can be fund in Appendix B.

Table 7.2: Initial set of parameters of STA/LTA algorithm

Short Term Average/Long Term Average (STA/LTA)			
DBDETECTPAR CODE	**NAME**	**STA (sec)**	**LTA (sec)**
D	High Frequency	1	10
E	Emergent	10	60

Table 7.3: Second set of parameters of STA/LTA algorithm

Short Term Average/Long Term Average (STA/LTA)			
DBDETECTPAR CODE	**NAME**	**STA (sec)**	**LTA (sec)**
EV1	Event 1	4	40
EV2	Event2	8	80
EV3	Event 3	16	160

The algorithm computes different types of detectors (depending of the set of parameters) to identify possible triggering in local events. The STA/LTA was tested in reference stations R11A, TX31 and ANMO first to obtain preliminary outcomes. All these parameters were adjusted to different windows lengths and having a critaria of 3.5 for the average of the signal. This algorithm was applied to all vertical component seismograms. A linear regression was calculated from all the results gathered in order to have a better understanding of the behavior/performance of the results. The graphs 7.3 to 7.8 show results for the most suitable detector, (Ev2 detector), displaying detections plotted using a 24-hour window versus number of detectors identifed. Results are shown in the following figures.

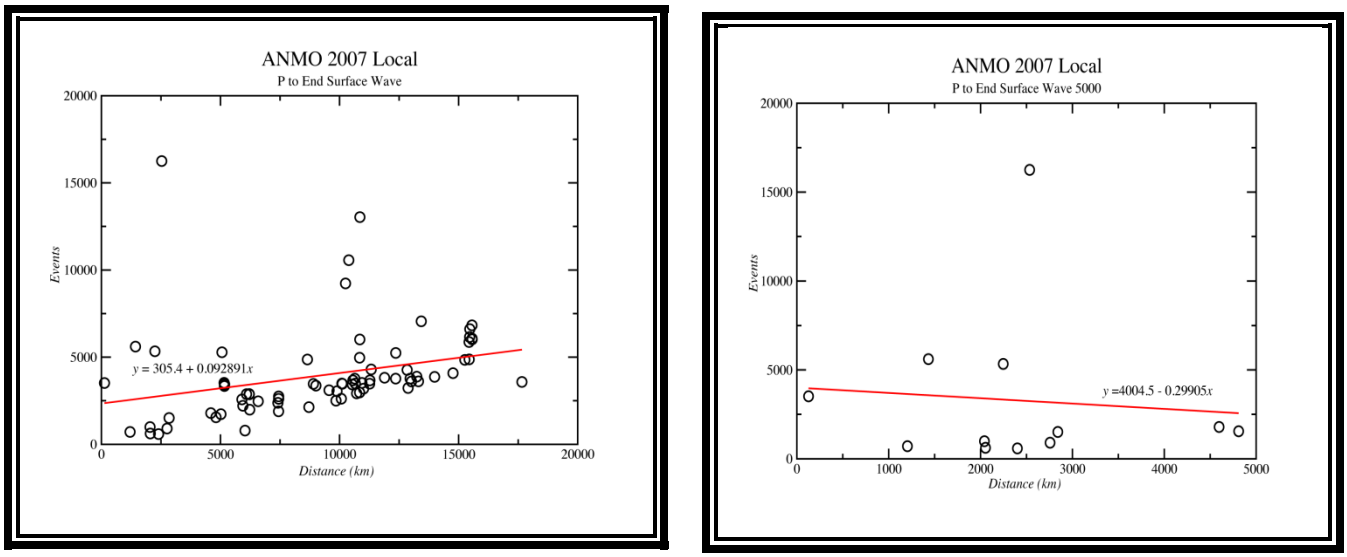

Figure 7.3: Reference station ANMO. Plots showing number of events recorded for local events versus station distance. Data covers all 2007. Red line shows the regression value calculated for the signal analysis. (a) Analysis from the beginning of the *P*-wave to end of surface wave. (b) Same data but now, data has been reduced to 5000 km from the station.

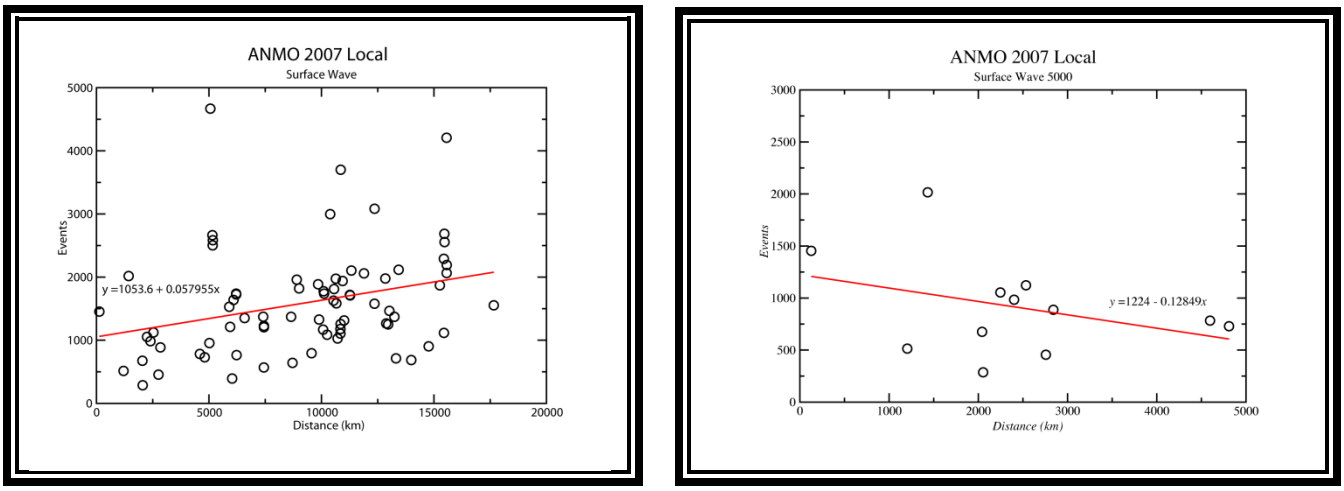

Figure 7.4: Reference station ANMO. Plots showing number of events recorded for local events versus station distance. Data covers year 2007. Red line shows the regression value calculated for the signal analysis. (a) Analysis from the beginning of the surface-wave to end of surface wave. (b) Same data but now, data has been reduced to 5000 km from the station.

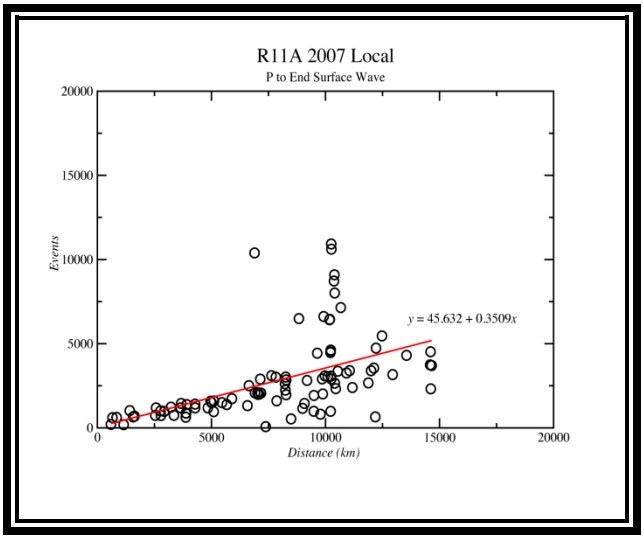

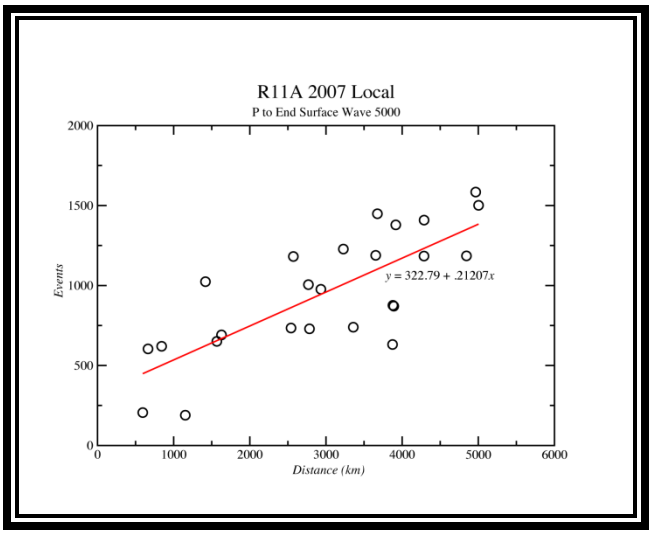

Figure 7.5: Reference station R11A. Plots showing number of events recorded for local events versus station distance. Data covers all 2007. Red line shows the regression value calculated for the signal analysis. (a) Analysis from the beginning of the *P*-wave to end of surface wave. (b) Same data but now, data has been reduced to 5000 km from the station.

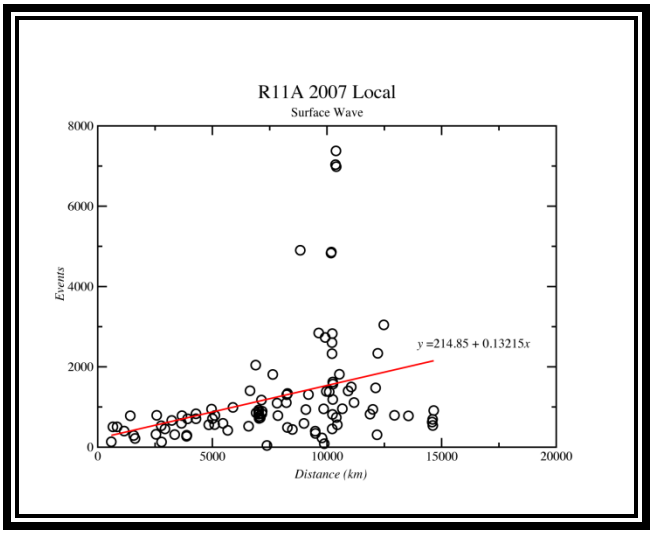

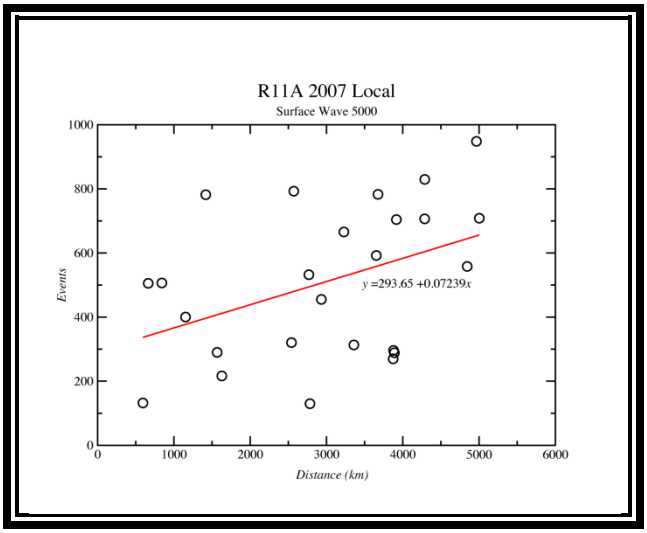

Figure 7.6: Reference station R11A. Plots showing number of events recorded for local events versus station distance. Data covers year 2007. Red line shows the regression value calculated for the signal analysis. (a) Analysis from the beginning of the surface-wave to end of surface wave. (b) Same data but now, data has been reduced to 5000 km from the station.

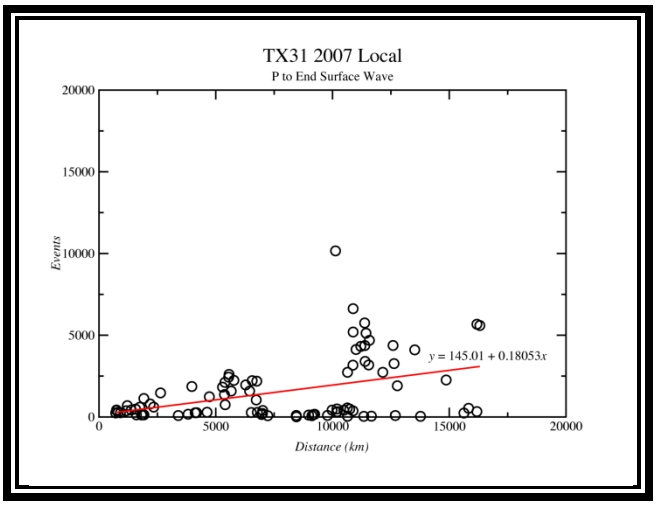

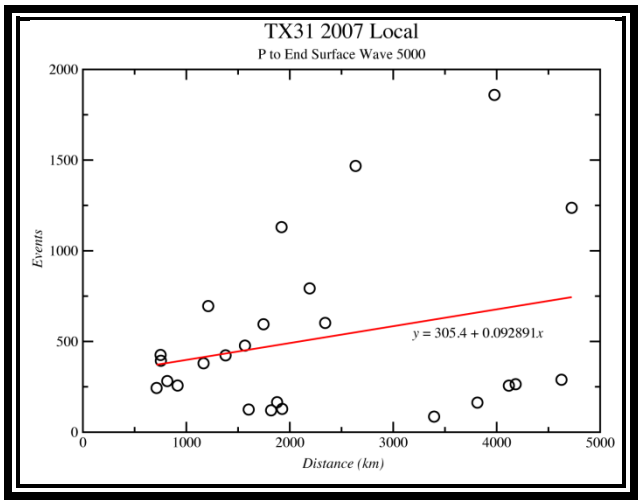

Figure 7.7: Reference station TX31. Plots showing number of events recorded for local events versus station distance. Data covers all 2007. Red line shows the regression value calculated for the signal analysis. (a) Analysis from the beginning of the *P*-wave to end of surface wave. (b) Same data but now, data has been reduced to 5000 km from the station.

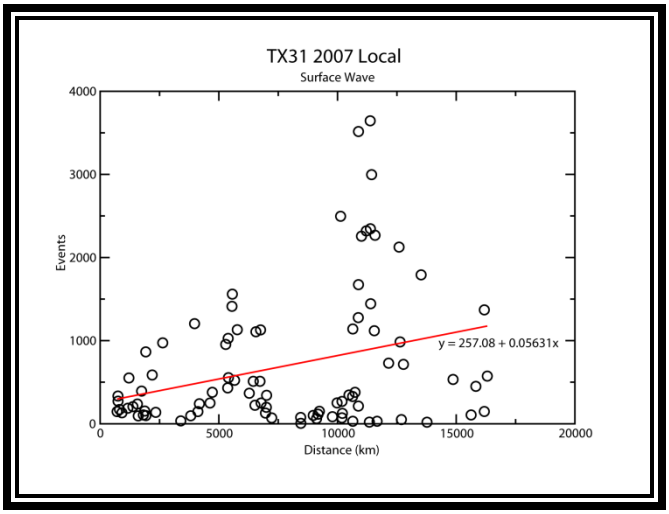

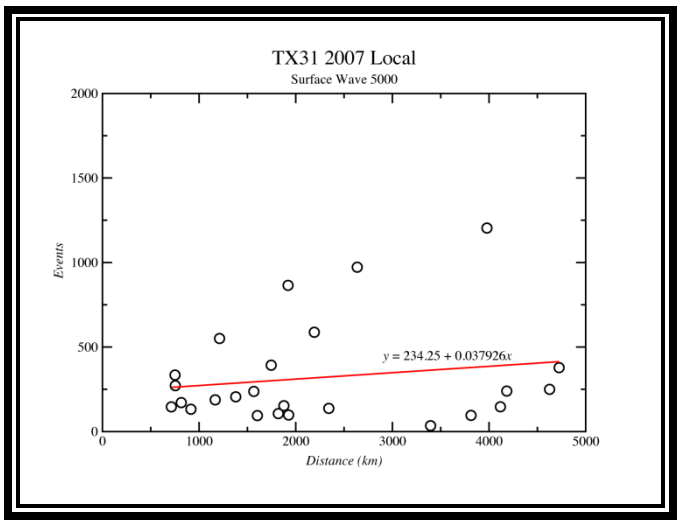

Figure 7.8: Reference station R11A. Plots showing number of events recorded for local events versus station distance. Data covers year 2007. Red line shows the regression value calculated for the signal analysis. (a) Analysis from the beginning of the surface-wave to end of surface wave. (b) Same data but now, data has been reduced to 5000 km from the station.

Ev2 shows a more accurate response for possible triggered events. The number of events detected shows events with a distance in average of 80 km from the station, given a better prediction of local events identified for each station. By using this approach we are eliminating any possible aftershocks or high frequency noise that could be erroniously counted as triggered. For example, detector Ev1, shows detections close to the stations (~10-30 km) that could be easily mistaken with static stresses and not remotely triggered. To quantify and minimize uncertainties, we have neglected information greater than 100 events near the station and have narrow the station distance to 5000 km. from each station.

One of the challenges is to determine what noise could be contaminating our results. We stack our detections on hourly bins for all three stations, and plot the number of detections for each detection type (Figures 7.9-7.11). While analyzing the results from the reference stations, we note a significant increments of detections during the 12 and 15 hour. This increase in detections could possible be an indication of man-made noise captured and recorded by the seismic stations (city noise as traffic, contructions, etc). Further studies could be conducted to identified if certain time ranges could influence any changes in frequency spectra recorded at seismic stations.

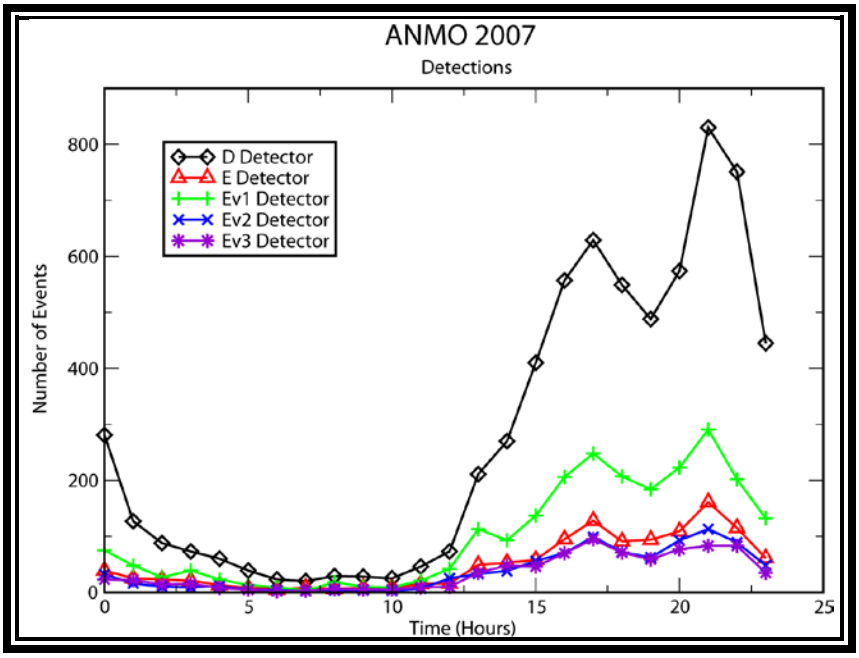

Figure 7.9: Reference station ANMO. Plot shows the different algorithm parameters and their performance. Data evaluated over one year period (2007). Data plotted in a 24-hour window versus number of events.

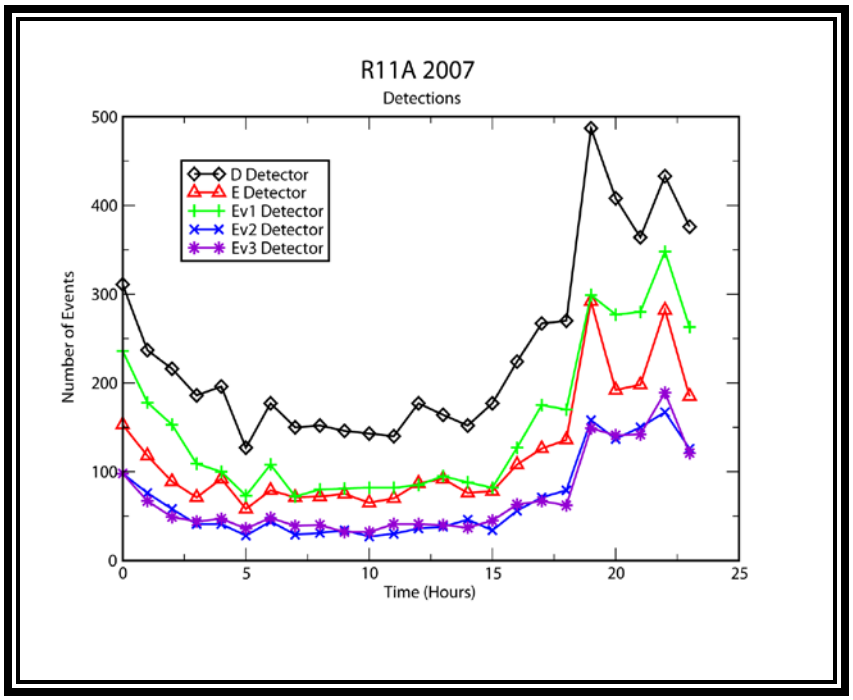

Figure 7.10: Reference station R11A. Plot shows the different algorithm parameters and their performance. Data evaluated over one year period (2007). Data plotted in a 24-hour window versus number of events.

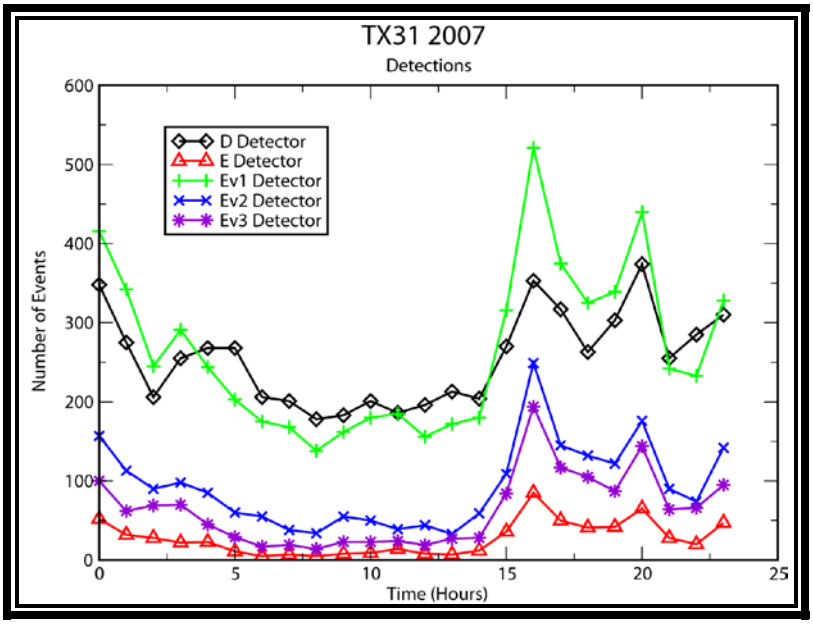

Figure 7.11: Reference station TX31. Plot shows the different algorithm parameters and their performance. Data evaluated over one year period (2007). Data plotted in a 24-hour window versus number of events.

7.2 SEGMENT TWO. FEATURE ANALYSIS

Segment two of this investigation deals with the application of the algorithm applied to five events that provide a full range of seismic wave amplitudes and orientations across the footprint of the USArray seismic stations. These events are two teleseismic megatrust events, the Maule, Chile on February 27, 2010 (M 8.8), Tohoku-Oki, Japan on March 11, 2011 (M 9.0); two large strike-slip earthquakes, West coast of northern Sumatra on April 11, 2012 (M 8.2 and 8.6); and two large regional events, the strike-slip Baja California, Mexico on April 04, 2010 (M 7.2) earthquake, and the normal fault Wells Nevada, U.S., on February 21, 2008 (M 6.0).

7.2.1 –Seismic Network and Seismic Stations

This investigation has been focused on using the Transportable Array (TA) network. This seismic network has the capability of generate all the information necessary due to its features and extensive coverage. For all of the events, Table 7.2.1 shows the description of the network and, table 7.2.2 shows a detail list of all the stations that are covered under the TA's network.

Table 7.4: Seismic Network

NETWORK CODE	NETWORK NAME	NETWORK OPERATOR
TA	USArray Transportable Array	Earthscope Project (IRIS)

Table 7.5: List of Transportable Array (TA) stations.

TRANSPORTABLE ARRAY (TA) STATIONS								
058A	351A	959A	F31A	I34A	L38A	O39A	S44A	W45A
059A	352A	A04D	F32A	I35A	L39A	O40A	S45A	W46A
059Z	353A	A31A	F34A	I36A	L40A	O41A	S46A	W47A
060A	355A	A32A	F35A	I37A	L41A	O42A	S48A	W48A
109C	356A	A33A	F36A	I38A	L42A	O43A	SFIN	WHTX
121A	357A	ABTX	F37A	I39A	L43A	O44A	SPMN	X39A
140A	435B	B05D	F38A	I40A	L44A	O45A	SUSD	X40A
141A	441A	B31A	F39A	I41A	M02C	O47A	T25A	X41A
142A	442A	B32A	F40A	I42A	M04C	O56A	T39A	X42A
143A	443A	B33A	F41A	I43A	M33A	P37A	T40A	X43A
144A	444A	B34A	F42A	J01D	M34A	P38A	T41A	X44A
145A	445A	B35A	F43A	J05D	M35A	P39B	T42A	X45A
146A	446A	BGNE	F44A	J31A	M36A	P40A	T43A	X46A
147A	447A	C31A	F45A	J32A	M37A	P41A	T44A	X47A
148A	448A	C32A	F46A	J33A	M38A	P42A	T45A	X48A
149A	449A	C33A	G03D	J34A	M39A	P43A	T46A	X49A
150A	450A	C34A	G05D	J35A	M40A	P44A	T47A	X50B
151A	451A	C35A	G31A	J36A	M41A	P45A	T48A	X51A
152A	452A	C36A	G32A	J37A	M42A	P46A	TIGA	X52A
153A	453A	C37A	G33A	J38A	M45A	P47A	TOLK	X53A
154A	454A	C38A	G34A	J39A	M46A	Q24A	TPFO	Y12C
155A	455A	C39A	G35A	J40A	M54A	Q37A	TUL1	Y22D
156A	456A	C40A	G36A	J41A	M65A	Q38A	U39A	Y40A
214A	457A	D03D	G38A	J42A	MDND	Q39A	U40A	Y41A
240A	541A	D04D	G39A	J43A	MSTX	Q40A	U41A	Y42A
241A	542A	D31A	G40A	K02D	N02D	Q41A	U42A	Y43A
242A	543A	D32A	G41A	K04D	N23A	Q42A	U43A	Y44A
244A	544A	D33A	G42A	K22A	N33A	Q43A	U44A	Y45A
245A	545A	D34A	G43A	K31A	N34A	Q44A	U44B	Y46A
246A	546A	D35A	H04D	K32A	N35A	Q46A	U45A	Y47A
247A	552A	D36A	H17A	K33A	N36A	Q47A	U46A	Y48A
248A	553A	D37A	H31A	K34A	N37A	R11A	U47A	Y49A
249A	554A	D41A	H32A	K35A	N38A	R38A	U48A	Y50A
250A	555A	E04D	H33A	K36A	N39A	R39A	V39A	Y51A
251A	556A	E31A	H34A	K37A	N40A	R40A	V40A	Y52A
252A	557A	E32A	H35A	K38A	N41A	R41A	V41A	Y54A
253A	645A	E33A	H36A	K39A	N42A	R42A	V42A	Z40A
254A	646A	E34A	H37A	K40A	N43A	R43A	V43A	Z41A
255A	655A	E35A	H38A	K41A	N44A	R44A	V44A	Z42A
256A	656A	E36A	H39A	K42A	N45A	R45A	V45A	Z43A
257A	657A	E37A	H40A	K43A	N46A	R46A	V46A	Z44A
341A	658A	E38A	H42A	KMSC	N54A	R47A	V47A	Z45A
342A	757A	E39A	H43A	L02D	N59A	R48A	V48A	Z46A
343A	758A	E40A	I02D	L04D	O02D	S22A	W18A	Z47A
344A	833A	E41A	I03D	L32A	O03D	S38A	W39A	Z48A
345A	857A	E42A	I04A	L33A	O33A	S39A	W40A	Z49A
347A	858A	E43A	I05D	L34A	O34A	S40A	W41B	Z50A
348A	859A	E44A	I31A	L35A	O35A	S41A	W42A	Z51A
349A	957A	E45A	I32A	L36A	O37A	S42A	W43A	Z52A
350A	958A	F05D	I33A	L37A	O38A	S43A	W44A	Z53A

7.2.2 –Love and Rayleigh Wave Analysis

It has been assumed that the passing of seismic waves will change critical stress forces and trigger dynamically. To demonstrate that triggering occurs during the passage of surface waves, we obtained, for all stations, their respective latitude, longitude and azimuth. Also, for each detection, the respective latitude and longitude, was obtained and created station-distance and time-distance relationships. We have assumed that the typical velocity for Love waves to be V_L= 4.3 km/s and for Rayleigh waves to be V_R= 3.5 km/s. Then, we added the number of detections obtained along the group velocity curves for Love and Rayleigh waves creating time-reduced histograms. The time-reduced values were calculated by multiplying the distance of each station in degrees by 111.19 (value for a degree) to obtain the distance in km. These will show that the activity that increases with the arrival of seismic waves is more confidentially identified as triggered. To eliminate high frequency detections from noisy stations caused by external factors, we have delimited our detection frequency number to be at a maximum of 60 events for each station (when available); this must also restrict the number of possible aftershocks that could be erroneous counted as triggered. To test the significance of the number of detections, we computed the mean of all the events that have been separated in the 300 seconds bins before and after the main event. Approximating a Poisson distribution, we computed the confidence intervals for each of the events.

I noted that the triggered earthquakes occurred during the first few cycles of the Love waves, and occurred again during the large amplitude Rayleigh waves.

However, I only examine the continuous data within several hours before and after the *P*-arrivals of each earthquake, to assure continuous recording, this time frame has been sufficient to calculate the time velocities for the respective Love and Rayleigh waves for each of the events.

Our modeling results show that the triggering potential for the Love waves are larger than for those of the Rayleigh waves (Gonzales-Huizar and Velasco, 2012). Locally triggered events during the

Love wave generally have larger amplitudes than the local events during Rayleigh waves. Nonetheless, results shows clear dynamic triggering for the two types of surface waves. This could be associated to the fact that all the events that were analyzed for this project has been of reasonable magnitudes or in close distance to dense seismic stations.

Another characteristic that was recognized in our study was that for our events of M>8.0 the average depth was about ~24 km, while for those of magnitude between 6.0< M >7.5, it was found to be between the range of ~5 km. According to Chao and Peng (2009), the reductions of seismic group velocities are generally on the order of a few percent for large nearby earthquakes, meaning that at shallow depths it could be found a reduction of seismic velocities in the crust during the passage of large amplitude surface waves. That means that deep earthquakes can only generate long-period fundamental Rayleigh waves, whereas shallow earthquakes generate broader-band surface waves. This information can also be a factor leading to the result of triggered events found at certain ranges with an increase or decrease in number of events. Many of these possible events are not found in seismic earthquake catalogs. For this reason, we do not know their exact location and/or focal mechanism.

In a recent study Pollitz (2012), stated that triggered events are not preferentially located in the near field, where dynamic strain magnitudes are high, but rather are distributed uniformly over the globe. His conclusion was founded after a study performed for the Sumatra earthquake following almost an equivalent method like the one we used. They also found that small events triggered by passage of seismic waves, whether instantaneous or delayed, depend more than dynamic strain amplitude. His results shown events that produced earthquake nucleation recorded as far as Baja California, Mexico. Nonetheless, to produce earthquake nucleation, the stress changes from seismic waves must arrange satisfactorily with the faults that they pass through.

Different surface wave amplitudes carry different levels of energy. All these energies carry distinctive characteristics and interact producing specific ground shakings for specific fault orientations.

Different attributes need to be explored for future studies, such as peak amplitudes, frequency content, the amplitude associated with each frequency, energy content, energy carried by ground shaking at each frequency band and/or the entire duration of strong shakings. Finally, attenuation is a key feature while dealing with surface waves, the earth itself acts as a natural big filter.

Baja California Earthquake

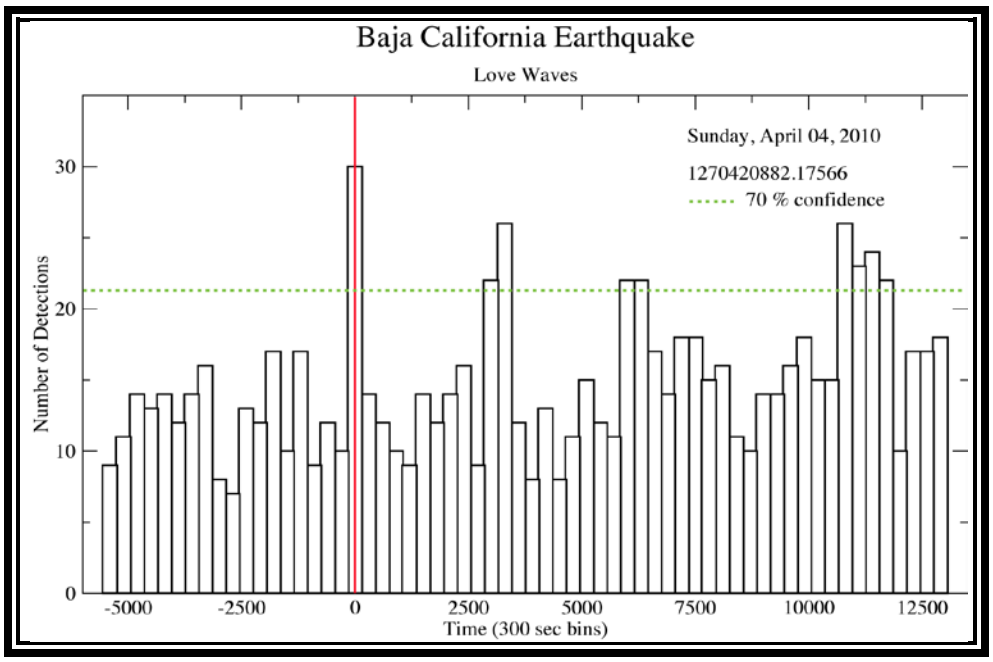

Figure 7.12: Baja California, Mexico earthquake. Time reduced histogram for Love wave group velocity (4.3 km/s) showing the number of possible triggered events grouped in 300 sec. bins.

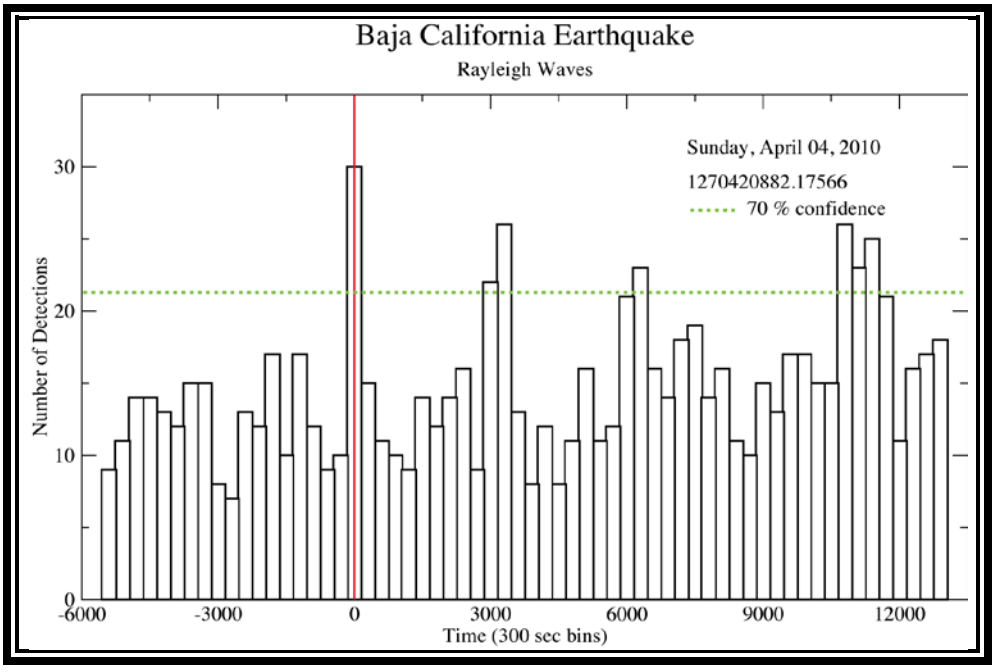

Figure 7.13: Baja California, Mexico earthquake. Time reduced histogram for Rayleigh wave group velocity (3.5 km/s) showing the number of possible triggered events grouped in 300 sec. bins.

The zero time line, on both histograms, corresponds to the arrival of Love- and Rayleigh- waves (respectively) (Figures 7.12 and 7.13). The green dashed line represents our confidence boundary, the closest to the boundary; the more confident we are that that bin has been triggered. The time of the main shock; for Baja California earthquake, is recorded at epoch time 1270420843.100 (22:40:43.100 UTC). The first detection for Love waves is found at epoch time 1270420882.17566 (22:41:22.17566 UTC) having ~39.1 seconds difference between the main shock and the first time arrival detected. Each window has an equivalent of 300 seconds bins and in each bin, the corresponding number of reduced-time events that fall into that specific time slot. This first detection was recorded in station P29A located in Atwood, KS.

I identified a clear shift in time delayed between Love and Rayleigh waves due to ground time velocity. There appears to be a general pattern of events identified/triggered along this event. The number of detections for this result, could possible better detect potential and temporal local changes associated with triggered activity.

Given that the distribution has a mean of 15 events per bin and a standard deviation of 5, the total number of detections laying between the mean minus standard deviation (10) and the mean plus standard deviation (20 events per bin), the number of detections between the standard deviation around the mean is 624. Considering that the total number of events is 908, my confidence of events detected is approximately 70%.

Chile Earthquake

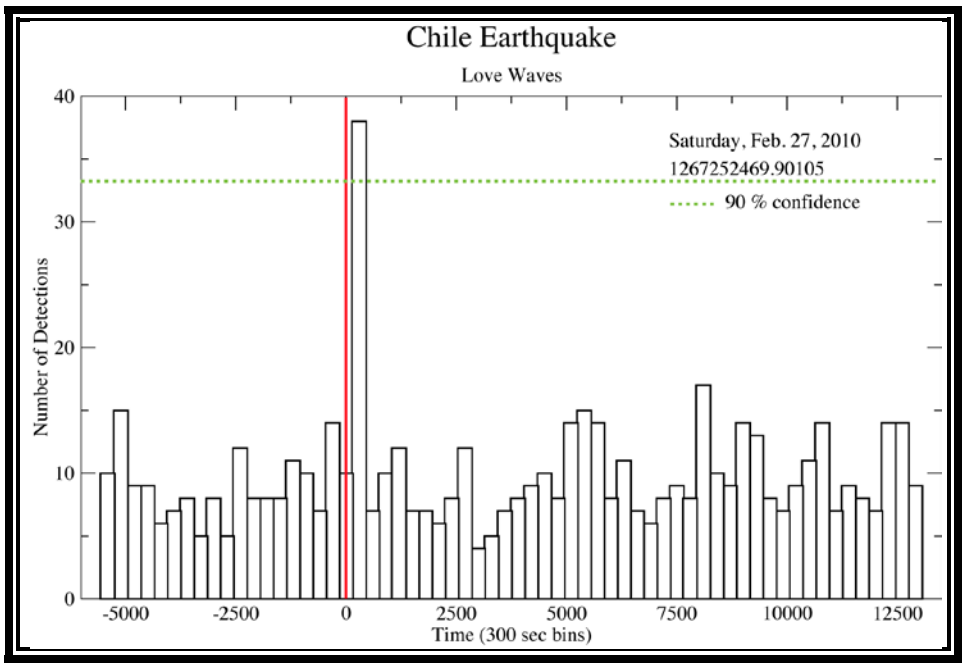

Figure 7.14: Chile earthquake. Time reduced histogram for Love wave group velocity (4.3 km/s) showing the number of possible triggered events grouped in 300 sec. bins.

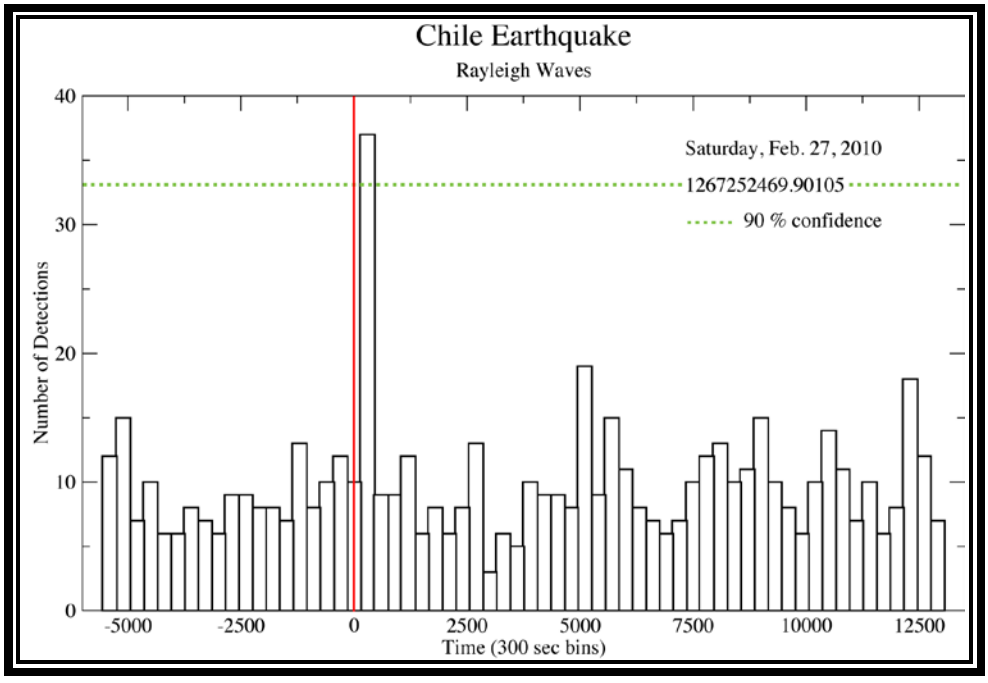

Figure 7.15: Chile earthquake. Time reduced histogram for Rayleigh wave group velocity (3.5 km/s) showing the number of possible triggered events grouped in 300 sec. bins.

The zero time line corresponds to the time of the Love- and Rayleigh-wave arrivals (respectively) (Figures 7.14 and 7.15). For the main shock, the time recorded in this case, is at 1267252451.530 (06:34:11.53000 UTC). The first detection for Love waves is at 1267252469.90105530 (06:34:29.90105 UTC) having ~18.1 seconds difference between waves, suggesting that most of the detections recorded are found immediately after the passage of the Love-wave signal. The difference in time of the recorded detector suggest that time may be a factor influencing frequencies of surface waves. Also, the radiation pattern may be a key feature in dynamic triggering. This first detection was recorded in station J20A situated in Shoshoni, WY.

Similar results were found for this particular event. There is a clear shift in time delayed between Love and Rayleigh waves and there is also a general pattern in detections. Given that the distribution has a mean of 10 events per bin and a standard deviation of 5, the total number of detections lying between the mean minus standard deviation (5) and the mean plus standard deviation (15 events per bin), the number of detections between the standard deviation around the mean is 549. Considering that the total number of events is 608, my confidence of events detected is approximately 90%.

Japan Earthquake

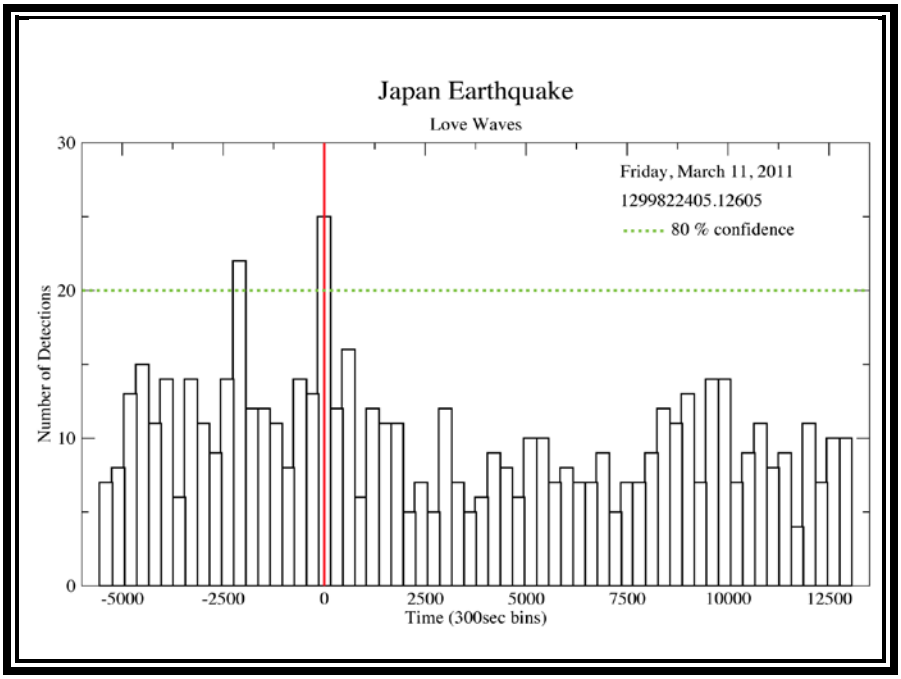

Figure 7.16: Japan earthquake. Time reduced histogram for Love wave group velocity (4.3 km/s) showing the number of possible triggered events grouped in 300 sec. bins.

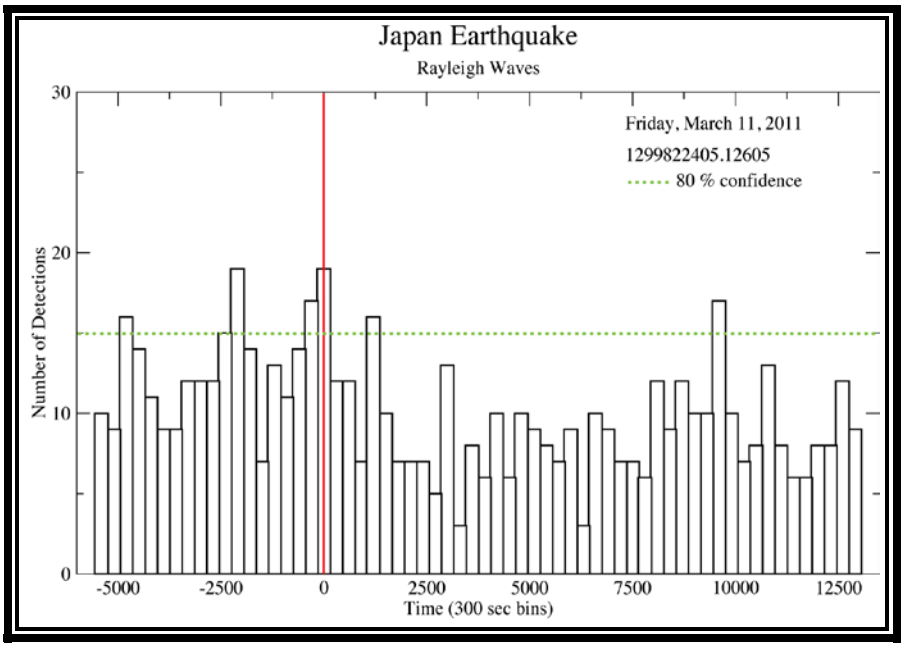

Figure 7.17: Japan earthquake. Time reduced histogram for Rayleigh wave group velocity (3.5 km/s) showing the number of possible triggered events grouped in 300 sec. bins.

The zero time line on both histograms corresponds to the time of Love- and Rayleigh-wave arrivals (respectively) (Figures 7.16 and 7.17). The time recorded for the main shock; in this case, is at 1299822384.120 (05:46:24.12000 UTC). The first detection of Love-waves is at 1299822405.12605 (05:46:45.12605 UTC) having ~20 seconds difference between the main shock and the first detector. This first detection was recorded in station L35A situated in Bielow Farm, Ricketts, IA.

I noticed from the results a reduction in the seismic activity right after the main shock. This could be due an alteration of potential energy accumulated in the tectonism. There is a sudden increase in detections recorded right after the passage of the main signal, having a similar response to the Chile event; in this case, the radiation pattern will be more horizontal compared with a vertical pattern of surface waves traveling around the globe. The difference between the Love- and Rayleigh- waves reduced time is clearly seen in the histograms above, both seismic waves, shown potential for triggering right after the main shock. This particular event also shows a reduction in overall detections; we have mentioned early that we have detected a particular pattern of triggered events for particular day-time, the Japan earthquake occurred on a Friday just before weekend possible reducing external noise.

Given that the distribution has a mean of 10 events per bin and a standard deviation of 4, the total number of detections lying between the mean minus standard deviation (6) and the mean plus standard deviation (14 events per bin), the number of detections between the standard deviation around the mean is 518. Considering that the total number of events is 620, my confidence of events detected is approximately 80%.

Nevada Earthquake

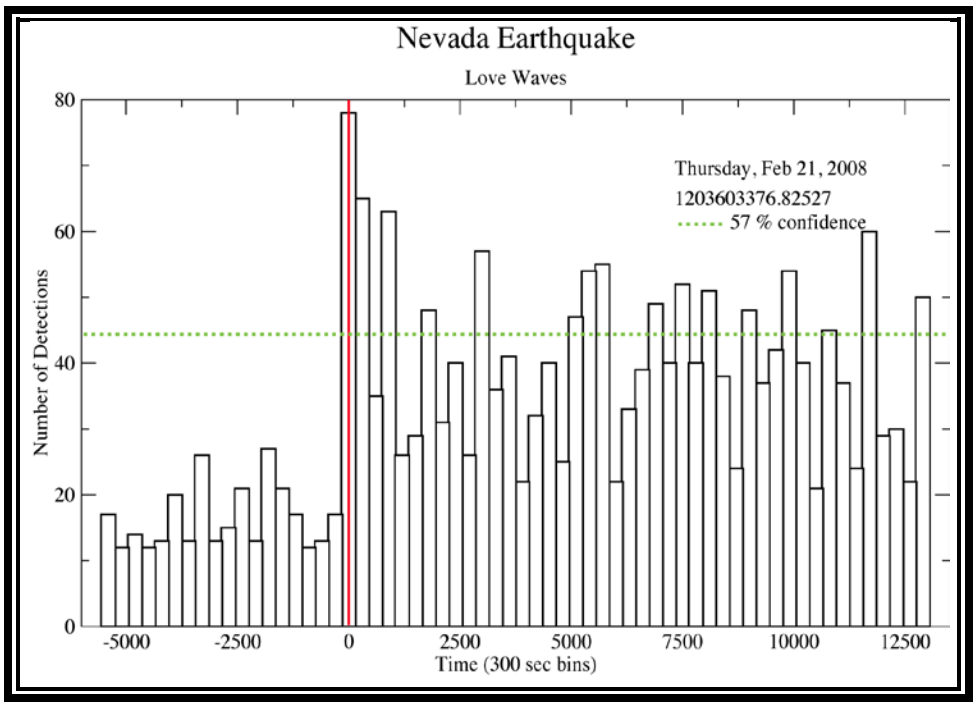

Figure 7.18: Nevada earthquake. Time reduced histogram for Love wave group velocity (4.3 km/s) showing the number of possible triggered events grouped in 300 sec. bins.

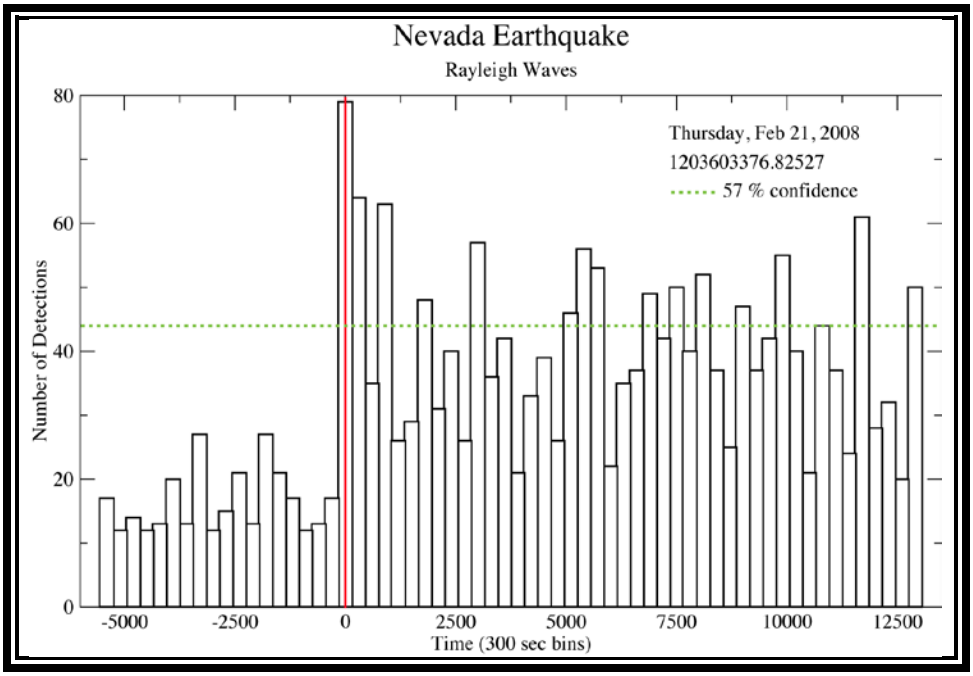

Figure 7.19: Nevada earthquake. Time reduced histogram for Rayleigh wave group velocity (3.5 km/s) showing the number of possible triggered events grouped in 300 sec. bins.

In this case, the time for the main shock is at 1203603362.710 (14:16:02.71000 UTC) (Figures 7.17 and 7.19). The first detection for Love-waves is at 1203603376.82527 (14:16:16082527 UTC) ~14 seconds difference between waves.

The event in Nevada, clearly show triggering of events, it also enhanced the seismic activity in the region, from an average of ~20 events prior to almost ~45 after the main shock. We can clearly notice a variation in the potential energy accumulated in the global tectonic environment. This earthquake, better predict potential and temporal local changes associated with a higher triggered activity. Fifteen bins over pass our confidence interval. One reason for having such number of detections could be attributed that that zone have been highly studied for last couple of years, having a dense network of seismograms deployed all over the region. For this specific event, it was necessary to decrease the study region associated to network stations; we just considered stations with a 500 km radius from the event to account just for local events produced by this event. This first Love–wave detection was recorded in station M11A situated in Holland Ranch, North Fork, NV.

Given that the distribution has a mean of 33 events per bin and a standard deviation of 16, the total number of detections laying between the mean minus standard deviation (17) and the mean plus standard deviation (49 events per bin), the number of detections between the standard deviation around the mean is 1164. Considering that the total number of events is 2073, my confidence of events detected is approximately 57%.

Sumatra Earthquake (M 8.6)

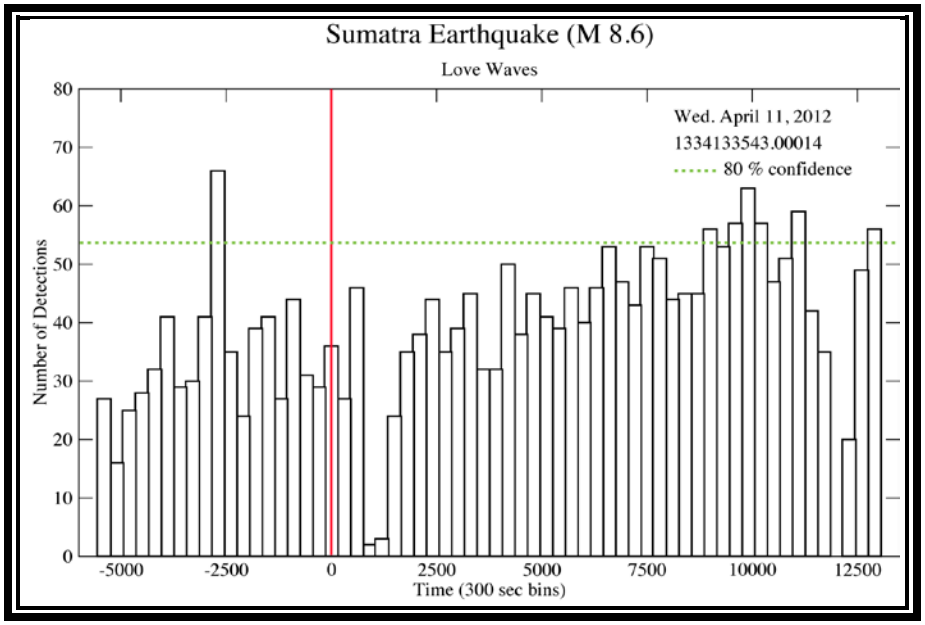

Figure 7.20: Sumatra earthquake (M 8.6). Time reduced histogram for Love wave group velocity (4.3 km/s) showing the number of possible triggered events grouped in 300 sec. bins.

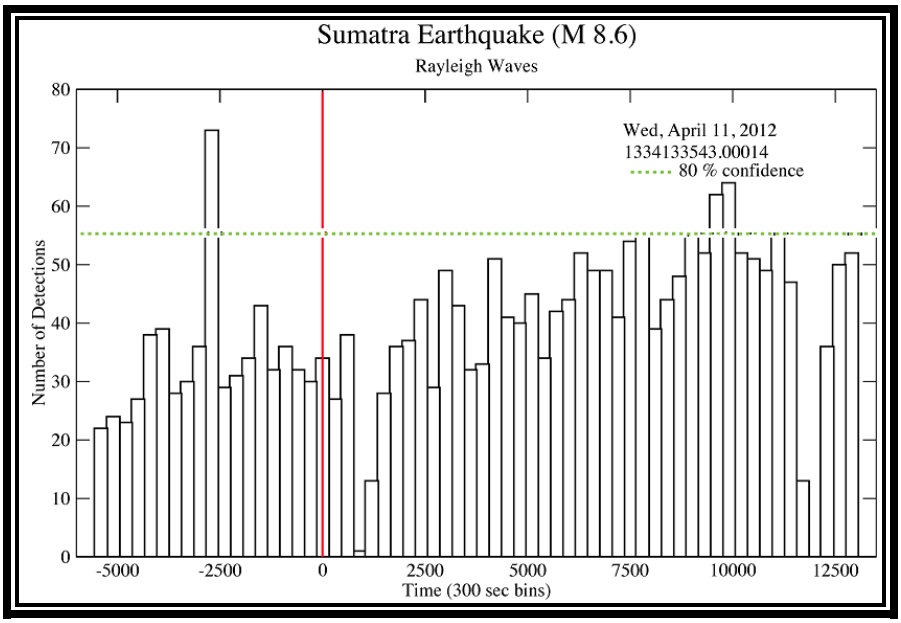

Figure 7.21: Sumatra earthquake (M 8.6). Time reduced histogram for Rayleigh wave group velocity (3.5 km/s) showing the number of possible triggered events grouped in 300 sec. bins.

In this case, the time for the main shock is at 1334133516.720 (08:38:36.72000 UTC) (Figures 7.20 and 7.21). The first detection for Love-waves is at 1334133543.00014 (08:39:03.00014 UTC) having ~26 seconds difference between them. This first Love-wave detection was recorded in station 447A situated in Lucedale, MS.

I noticed that the passage of seismic waves produced an instantaneous suppression or drop in seismic activity followed again by an increased in activity. We later see another suppression which suggests a possible cyclic sequence of suppression and enhancement in seismic activity. Additional triggered events at later times could escape our detection mechanism. Here, we also noticed the time delayed changes between Love and Rayleigh time velocities.

Given that the distribution has a mean of 39 events per bin and a standard deviation of 14, the total number of detections lying between the mean minus standard deviation (25) and the mean plus standard deviation (53 events per bin), the number of detections between the standard deviation around the mean is 1911. Considering that the total number of events is 2414, my confidence of events detected is approximately 80%.

Sumatra Earthquake (M 8.2)

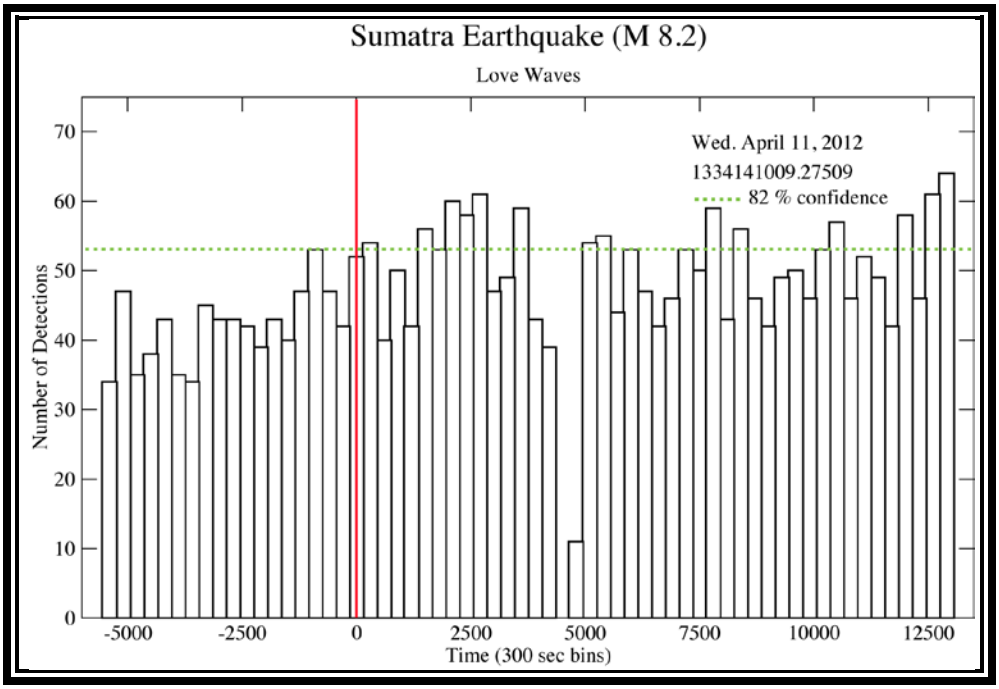

Figure 7.22: Sumatra earthquake (M 8.2). Time reduced histogram for Love wave group velocity (4.3 km/s) showing the number of possible triggered events grouped in 300 sec. bins.

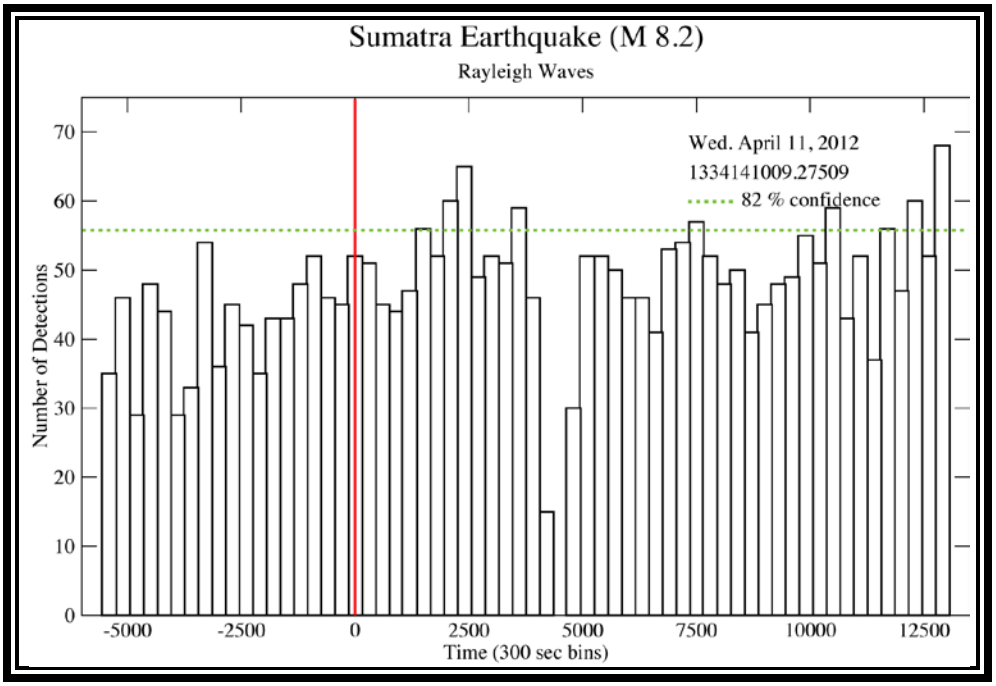

Figure 7.23: Sumatra earthquake (M 8.2). Time reduced histogram for Rayleigh wave group velocity (3.5 km/s) showing the number of possible triggered events grouped in 300 sec. bins.

.

For this event, the time for the main shock is at 1334140990.850 (10:43:10.85000 UTC) (Figures 7.22 and 7.23). The first detection for Love waves is found at 1334141009.27509 (10:43:29.27509 UTC) having ~18 seconds difference between the main shock and the first Love-wave time arrival. This first detection was recorded in station X52A situated in Dahlonega, GA.

For this event we found a sequence of enhancement-suppression-enhancement of detections which suggests that both of Sumatra earthquakes have a similar combination of (enhancement-suppression) behavior that we cannot see in other events. Another attribute for this event, is that there is only a difference of ~2 hours from each event, possible indicating that there were different or large amplitudes with short durations for a specific period of time.

Given that the distribution has a mean of 47 events per bin and a standard deviation of 11, the total number of detections lying between the mean minus standard deviation (36) and the mean plus standard deviation (58 events per bin), the number of detections between the standard deviation around the mean is 2374. Considering that the total number of events is 2887, my confidence of events detected is approximately 82%.

Chapter 8: Conclusions

Observations indicate that transient dynamic deformations trigger earthquakes, the physical mechanisms by which they do so, remain unknown. Here we presented a new analytical technique to test for the existence of and to estimate dynamic triggering detection.

The purpose of this investigation focused in studying the effects of surface waves properties in order to trigger earthquakes along their path. The method presented here is a simple and dynamic technique to investigate the effects of high magnitude earthquakes and the responses pre- and post-seismic recorded at different seismological stations to be capable of producing new earthquake nucleation far away from the main event. By analyzing surface waves (Love, Rayleigh), the opportunity to find events that could be hidden into the signal train has been determined by applying a high pass filter to the signal (~5 Hz); then, a STA/LTA algorithm has been applied to determine the number of occurrence of HFD's.

After analyzing five teleseismic events and using all the tools and resources that the USArray has implemented, the acquisition of high quality seismograms has been possible. The number of HFD's is a determinant factor to associate the passage of seismic surface waves to analytically address the correlation in detections obtained and compared them with the seismogram frequency content. This observation indicated that input wave amplitude plays an important role in controlling the triggering nucleation and the resulting amplitudes of the triggered events. Our results are consistent with the theory of dynamic triggering, in other words, triggered events, which are more likely to be located near the velocity strengthening of the Love wave are normally aseismic and can be driven by large dynamic stresses.

References

[Allaby, Ailsa and Allaby, Michael. Coulomb Failure Criterion. A Dictionary of Earth Sciences. 1999. Encyclopedia.com. 27 May. 2011 <http://www.encyclopedia.com>.]

[Anderson, J.G. et. Al. Seismicity in the western great Basin apparently triggered by the Landers, California earthquake, 28 June 1992. Bull. Seismol. Soc. Am. 84, 863-891 (1994).]

[Brodsky, E. E., E. Gordeev, and H. Kanamori. Landslide basal friction as measured by seismic waves, *Geophys. Res. Lett.*, 30(24), 2236. (2003).]

[Brodsky, E. E., Karakostas, V., Kanamori, H. A new observation of dynamically triggered regional seismicity: earthquakes in Greece following the August, 1999 Izmit, Turkey earthquake. Geophys. Res. Lett. 27, 2741-2744 (2000).]

[Chao, K. Peng, Z., 2009. Temporal changes of seismic velocity and anisotropy in the shallow crustinduced by the 1999 October 22 M6.4 Chia_Yi, Taiwan earthquake, Geophys. J. Int., 179, 1800-1816.]

[Eberhart-Phillips, D. et al. The 2002 Denali Fault earthquake, Alaska: A large magnitude, slip-partitioned event. Science 300, 1113-1118 (2003).]

[Goldstein, P., A. Snoke, (2005), "SAC Availability for the IRIS Community", Incorporated Institutions for Seismology Data Management Center Electronic Newsletter.]

[Goldstein, P., D. Dodge, M. Firpo, Lee Minner (2003) "SAC2000: Signal processing and analysis tools for seismologists and engineers, Invited contribution to "The IASPEI International Handbook of Earthquake and Engineering Seismology", Edited by WHK Lee, H. Kanamori, P.C. Jennings, and C. Kisslinger, Academic Press, London.]

[Gomberg, J., Bodin, p., Larson, K., Dragert, H. Earthquake nucleation by transient deformations caused by the M=7.9 Denally, Alaska, earthquake, Nature 427, 621-624 (2004).]

[Gomberg, J., Johnson, P. Dynamic triggering of earthquakes. Nature 437, 830 (2005).]

[Gonzalez-Huizar, H., and A. A. Velasco. Dynamic triggering: Stress modeling and a case study, *J. Geophys. Res.*, 116, B02304, doi:10.1029/2009JB007000 (2010).].

[Harris, R. A., Simpson, R. W., Reasenberg, P. A. Influence of static stress changes on earthquake locations in southern California. Nature 375, 221-224 (1995).]

[Harris, R. A., Simpson, R. W. In the shadow of the 1857-The effect of the great Ft. Tejon earthquake on subsequent earthquakes in southern California. Geophys. Res. Lett. 23, 229-232 (1996).]

[Harris, R. A. Introduction to special section: Stress triggers, stress shadows, and implications for seismic hazard. J. Geophys. Res. 103, 24347-24358 (1998).]

[Hill, D. P. et. Al. Seismicity in the western United States remotely triggered by the M 7.4 Landers, California, earthquake of June 28, 1992. Science 260, 1617-1623 (1993).]

[Hill, D. P. Dynamic stress, Coulomb failure, and remote triggering. Bull. Seismol. Soc. Am. 98, 66-92 (2008).]

[Husen, S., Wiemer, S., Smith, R. B. Remotely triggered seismicity in the Yellowstone National Park region by the 2002 Mw=7.9 Denali Fault Earthquake, Alaska. Bull. Seismol. Soc. Am. 94, S317-S331 (2004).]

[Husker, A. L., Brodsky, E. E. Seismicity in Idaho and Montana triggered by the Denali Fault Earthquake: A window into the geologic context for seismic triggering. Bull. Seismol.Soc. Am. 94, S310-S316 (2004).]

[Kilb, Deborah; Gomberg, Joan; Bodin, Paul. Triggering of earthquake aftershocks by dynamic stresses. Nature. Vol. 408. 570-574. (2000).]

[King, G.C.P., Stein, R. S., Lin, J. Static stress changes and the triggering of earthquakes. Bull. Seismol. Soc. Am. 84, 935-953 (1994).]
[Li, X., Cormier, V. F., Toksoz, M. N. Complex source process of the 17 August 1999 Izmit, Turkey, earthquake. Bull. Seismol. Soc. Am. 92, 267-277 (2002).]
[Lin, J., Stein, R. S. Stress triggering in thrust and subduction earthquakes and stress interaction between the southern San Andreas and nearby thrust and strike-slip faults. J. Geophys. Res. 109. (2004).]
[Parsons, T., and A. A. Velasco. On near-source earthquake triggering, *J. Geophys. Res.*, 114, B10307. (2009).]
[Parsons, T. Global Omori Law decay of triggered earthquakes: Large aftershocks outside the classical aftershock zone. J. Geophys. Res. 107, doi:10.1029/2001JB000646 (2002).]
[Pankow, K. L., Arabasz, W J., Pechmann, J. C., Nava, S. J. Triggered seismicity in Utah from the November 3, 2002, Denali Fault earthquake. Bull. Seismol. Soc. Am. 94, S332-S347 (2004).]
[Pollite, Fred F., et al. The 11 April 2012 east Indian Ocean earthquake triggered large aftershocks worldwide. Nature. Doi:10.1038/11504. (2012)]
[Prejean, S. G. et. Al. Remotely Triggered seismicity on the United States west coast following the M 7.9 Denali Fault earthquake. Bull. Seismol. Soc.Am. 94, S348-S359 (2004).]
[Rubenstein, J. L. et al, Non-volcanic tremor driven by large transient shear stresses. Nature 448, 579-582 (2007).]
[Seeber, L., J. G. Armbruster, W.-Y. Kim, N. Barstow, and C. Scharnberger. The 1994 Cacoosing Valley earthquakes near Reading, Pennsylvania: A shallow rupture triggered by quarry unloading, *J. Geophys. Res.*, 103(B10), 24,505–24,521. (1998)]
[Stein, R.S., King, G. C. P., Lin, J. Stress triggering of the 1994 M=6.7 Northridge, California, earthquake by its predecessors. Science 265, 1432-1435 (1994).]
[Steck, L., Velasco, A. A., Cogbill, A. H., Patton, H. J. Improving regional seismic event location in China. Pure Appl. Geophys. 158, 211-240 (2001).]
[Tibi, R., Wiens, D. A., Inoue, H. Remote triggering of deep earthquakes in the 2002 Tonga sequences. Nature. Vol. 424. 921-925. (2003).]
[Velasco, A. A., Ammon, C. J., Farrell, J., Pankow, K. Rupture directivity of the November 3, 2002 Denali Fault earthquake determined from surface waves. Bull. Seismol. Soc. Am. 94, S293-S299 (2004).]
[Velasco, A. A., Ammon, C. J., Lay, T. Empirical Green function deconvolutions of broadband surface waves: Rupture directivity of the 1992 Landers, California (Mw=7.3) earthquake. Bull. Seismol. Soc. Am. 84, 735-750 (1994).]
[Velasco, A.A., Hernandez, S., Parsons, T., Pankow, K. Global ubiquity of dynamic earthquake triggering. Nature. Vol. 1. 375-379. (2008).]
[West, M., Sanchez, J.J., McNutt, S. R. Periodically triggered seismicity at Mount Wrangell, Alaska, after the Sumatra earthquake. Science 308, 1144-1146 (2005).]

Appendix

APPENDIX A: INPUT FILES FOR SOD RECIPE.

```
<?xml version="1.0" encoding="UTF-8"?>
<sod>
   <eventArm>
      <eventFinder>
         <name>..</name>
         <dns>edu/iris/dmc</dns>
         <originTimeRange>
            <startTime>99990101T11:59:59.000Z</startTime>
            <endTime>99990101T11:59:59.000Z</endTime>
         </originTimeRange>
         <magnitudeRange>
            <min> M </min>
         </magnitudeRange>
         <catalog> TYPE </catalog>
      </eventFinder>
      <printlineEventProcess/>
   </eventArm>
    <networkArm>
      <networkFinder>
         <name> Network </name>
         <dns>edu/iris/dmc</dns>
      </networkFinder>
         <networkOR>
          </networkOR>
         <bandCode> BAND </bandCode>
         <printlineChannelProcess/>
   </networkArm>
   <waveformVectorArm>
      <originOffsetRequest>
            <beginOffset>
              <unit>HOUR</unit>
              <value>-5</value>
            </beginOffset>
            <endOffset>
              <unit>HOUR</unit>
              <value>5</value>
            </endOffset>
      </originOffsetRequest>
      <fixedDataCenter>
         <name>IRIS_DataCenter</name>
         <dns>edu/iris/dmc</dns>
      </fixedDataCenter>
```

```
      <someCoverage/>
      <printlineSeismogramProcess/>
      <sacWriter/>
         <merge/>
      <rMean/>
      <rTrend/>
         <taper>
            <width>.05</width>
            <type>HANNING</type>
</taper>
         <taper/>
      <vectorTrim/>
         <rotateGCP/>
         <sacWriter>
         <workingDir> DIR </workingDir>
            <phaseTimeHeader>
                <model>ak135</model>
                   <phaseName>ttp</phaseName>
                   <tHeader>a</tHeader>
         </phaseTimeHeader>
      </sacWriter>
      <legacyExecute>
         <command>echo Sod saved this file</command>
      </legacyExecute>
   </waveformVectorArm>
</sod>
```

APPENDIX B: INPUT FILES FOR STA/LTA ALGORITHM.

```
#       Parameter files for dbdetect
#       Following are required and are used as overall defaults
ave_type        rms                     # Method for averaging (rms or filter)
sta_twin        1.0                     # short term average time window
sta_tmin        1.0                     # short term average minimum time for average
sta_maxtgap     0.5                     # short term average maximum time gap
lta_twin        10.0                    # long term average time window
lta_tmin        5.0                     # long term average minimum time for average
lta_maxtgap     4.0                     # long term average maximum time gap
nodet_twin      1.0                     # no detection if on time is less than this
pamp            500.0                   # plot amplitude
thresh          3.5                     # detection SNR threshold
threshoff       2.0                     # detection-off SNR threshold
det_tmin        10.0                    # detection minimum on time
det_tmax        100.0                   # detection maximum on time
h               0                       # plot channel height in pixels
filter          BW 1 4 20 4             # default filter
iphase          D                       # default iphase for detections
process_twin    500.0                   # data is processed in hunks of this duration

#       At least one default band must be set up in the bands table
#       Parameter values override default values above for each band
bands   &Tbl{
        &Arr{
                sta_twin        1.0
                sta_tmin        1.0
                sta_maxtgap     0.5
                lta_twin        10.0
                lta_tmin        5.0
                lta_maxtgap     4.0
                pamp            500.0
                filter          BW 5.0 4 0 0
                iphase          D
        }
          &Arr{
                sta_twin        10.0
                lta_twin        60.0
                filter          BW 5.0 4 0 0
                iphase          E
        }
          &Arr{
                sta_twin        4.0
                sta_tmin        4.0
                sta_maxtgap     0.5
                lta_twin        40.0
                lta_tmin        30.0
```

```
                lta_maxtgap     2.0
                pamp            500.0
                filter          BW 5.0 4 0 0
                iphase          Ev1
    }
        &Arr{
                sta_twin        8.0
                sta_tmin        8.0
                sta_maxtgap     0.5
                lta_twin        80.0
                lta_tmin        60.0
                lta_maxtgap     2.0
                pamp            500.0
                filter          BW 5.0 4 0 0
                iphase          Ev2
}
        &Arr{
                sta_twin        16.0
                sta_tmin        16.0
                sta_maxtgap     0.5
                lta_twin        160.0
                lta_tmin        100.0
                lta_maxtgap     2.0
                pamp            500.0
                filter          BW 5.0 4 0 0
                iphase          Ev3
        }
}

#       At least one data channel must be specified in the station channel table
stachans        &Tbl{
       .*       BHZ | 00BHZ | 10BHZ | HHZ | 00HHZ | 10HHZ
}
#    channels to reject in the processing
    reject &Tbl{ }
```

APPENDIX C: INPUT FILES FOR SAC MACRO

```
cut off
xlim off
setbb ofile $1$-env
getbb ofile
r $1
hilbert
sqr
w j1
r
sqr
addf j1
sqrt
w %ofile
```

Vita

Ibrahim Cerda was born on April 10, 1976 in Cd. Juarez, Chihuahua, Mexico. The second son of Jose Luis Cerda, Ms and Elvia Solis de Cerda, he graduated from The University of Texas at El Paso with a Bachelor of Science degree in Electrical and Computing Engineering in the summer of 2004. A second Bachelor of Science degree in Environmental Science with a concentration in Geology, in the spring of 2010.

In the summer of the same year, he enrolled in the Geophysics graduate program at The University of Texas at El Paso, having as a mentor, graduate and thesis advisor professor Aaron A. Velasco, PhD.

Permanent address: Lakehurst Dr.
El Paso, Texas, 79912

This thesis was typed by Ibrahim Cerda.